The OceanFlux Greenhouse Gases methodology for deriving a sea surface climatology of CO2 fugacity in support of air-sea gas flux studies

Ocean Sci., 11, 519–541, 2015
www.ocean-sci.net/11/519/2015/
doi:10.5194/os-11-519-2015

Ocean Science
Open Access

The OceanFlux Greenhouse Gases methodology for deriving a sea surface climatology of CO_2 fugacity in support of air–sea gas flux studies

L. M. Goddijn-Murphy[1], D. K. Woolf[2], P. E. Land[3], J. D. Shutler[4], and C. Donlon[5]

[1]ERI, University of the Highlands and Islands, Ormlie Road, Thurso, UK
[2]ICIT, Heriot-Watt University, Stromness, UK
[3]Plymouth Marine Laboratory, Prospect Place, Plymouth, UK
[4]University of Exeter, Centre for Geography, Environment and Society, Penryn, Cornwall, UK
[5]European Space Agency/ESTEC, Noordwijk, the Netherlands

Correspondence to: L. M. Goddijn-Murphy (lonneke.goddijn-murphy@uhi.ac.uk)

Received: 27 June 2014 – Published in Ocean Sci. Discuss.: 28 July 2014
Revised: 09 June 2015 – Accepted: 10 June 2015 – Published: 08 July 2015

Abstract. Climatologies, or long-term averages, of essential climate variables are useful for evaluating models and providing a baseline for studying anomalies. The Surface Ocean CO_2 Atlas (SOCAT) has made millions of global underway sea surface measurements of CO_2 publicly available, all in a uniform format and presented as fugacity, f_{CO_2}. As f_{CO_2} is highly sensitive to temperature, the measurements are only valid for the instantaneous sea surface temperature (SST) that is measured concurrently with the in-water CO_2 measurement. To create a climatology of f_{CO_2} data suitable for calculating air–sea CO_2 fluxes, it is therefore desirable to calculate f_{CO_2} valid for a more consistent and averaged SST. This paper presents the OceanFlux Greenhouse Gases methodology for creating such a climatology. We recomputed SOCAT's f_{CO_2} values for their respective measurement month and year using monthly composite SST data on a $1° \times 1°$ grid from satellite Earth observation and then extrapolated the resulting f_{CO_2} values to reference year 2010. The data were then spatially interpolated onto a $1° \times 1°$ grid of the global oceans to produce 12 monthly f_{CO_2} distributions for 2010, including the prediction errors of f_{CO_2} produced by the spatial interpolation technique. The partial pressure of CO_2 (p_{CO_2}) is also provided for those who prefer to use p_{CO_2}. The CO_2 concentration difference between ocean and atmosphere is the thermodynamic driving force of the air–sea CO_2 flux, and hence the presented f_{CO_2} distributions can be used in air–sea gas flux calculations together with climatologies of other climate variables.

1 Background

1.1 Introduction

Observations demonstrate that dissolved CO_2 concentrations in the surface ocean have been increasing nearly everywhere, roughly following the atmospheric CO_2 increase but with large regional and temporal variability (Takahashi et al., 2009; McKinley et al., 2011). In general, tropical waters release CO_2 into the atmosphere, whereas high-latitude oceans take up CO_2 from the atmosphere. Accurate knowledge of air–sea fluxes of heat, gas and momentum is essential for assessing the ocean's role in climate variability, understanding climate dynamics, and forcing ocean/atmosphere models for predictions from days to centuries (Wanninkhof et al., 2009).

The European Space Agency OceanFlux Greenhouse Gases (GHG) project (http://www.oceanflux-ghg.org/) is an initiative to improve the quantification of air–sea exchanges of greenhouse gases such as CO_2. The project has developed data sets suitable for computation of gas flux climatology in which mean gridded values are computed from multiple measurements over different years. The gas flux calculation requires accurate values of gas transfer velocity, in addition to the concentrations of the dissolved gas above and

below the air–water interface (Liss and Merlivat, 1986). The project has relied heavily on the data sets successfully developed and maintained by the Surface Ocean CO_2 Atlas (SOCAT, Bakker et al., 2014; Pfeil et al., 2013; Sabine et al., 2013). SOCAT has collated and carefully quality controlled the largest collection of ocean CO_2 observations providing data in an agreed and controlled format for scientific activities. Recognising that some groups may have difficulty working with millions of measurements, the SOCAT gridded product (Sabine et al., 2013) was then generated to provide a robust, regularly spaced f_{CO_2} product with minimal spatial and temporal interpolation. This gridded data set is useful for evaluating models and for studying and characterising f_{CO_2} variations within regions in a format that is easy to exploit. In this paper we present the OceanFlux-GHG methodology for creating a climatology of f_{CO_2} suitable for use in air–sea gas flux studies.

Gas concentrations of CO_2 in the upper ocean can be derived from SOCAT's underway sea surface measurements of fugacity, f_{CO_2} (p_{CO_2} adjusted to account for the fact that the gas is not ideal regarding molecular interactions between the gas and the air). The aquatic CO_2 concentration can be expressed as the product of f_{CO_2} and solubility of CO_2; the product of CO_2 concentration difference and gas transfer velocity, k, then gives us the air–sea gas flux. Different authors of CO_2 ocean–atmosphere gas flux products use either a mean value of f_{CO_2} (e.g. Schuster et al., 2009; Sabine et al., 2013) or p_{CO_2} (e.g. Takahashi et al., 2002, 2009; Landschützer et al., 2013; Jones et al., 2012; Rödenbeck et al., 2013) within a grid box for a particular measurement month and year. Many studies have used the p_{CO_2} climatology of Takahashi et al. (2002, 2009) as a basis to estimate their own air–sea fluxes (e.g. Kettle et al., 2005, 2009; Fangohr and Woolf, 2007; Land et al., 2013). The data sets from Takahashi et al. (2002, 2009) and Sabine et al. (2013) are calculated using in situ SST obtained at depth, SST_{depth}. In situ f_{CO_2} is derived from f_{CO_2} measured in the shipboard equilibrator using the difference between the temperature of sea water in the equilibrator and SST_{depth}. Because f_{CO_2} is highly sensitive to temperature fluctuations, an instantaneous measurement of f_{CO_2} is only really valid for its concurrent in situ SST_{depth} measurement. Takahashi et al. (2009) note there is a bias between the temperatures associated with the partial pressure measurements (and their gridded and interpolated values) and the SST_{depth} product used in their calculation of solubility (and thus fluxes). That inconsistency implies a bias between the upper ocean p_{CO_2} values with the true climatological mean values. They estimate a mean $+0.08\,^{\circ}C$ temperature difference, introducing a systematic bias of about $+1.3\,\mu atm$ in the mean surface water p_{CO_2} over all monthly mean values obtained in their study. They apply a correction to the global CO_2 flux on that basis. Takahashi et al. (2009) also acknowledge that by using SST_{depth} in their calculations, surface-layer effects could introduce systematic errors in the sea–air p_{CO_2} differences. Additional SST biases are also likely introduced by different measurement systems that measure SST at sea (Donlon et al., 2002), each with their own characteristic measurement biases.

All biases in SST, and hence in f_{CO_2}, contribute to uncertainties in the true monthly means of f_{CO_2}. Also for the purposes of calculating fluxes, each grid-cell value of fugacity must be paired with a SST value, such that temperature products are used consistently and correctly throughout the flux calculation. A true monthly mean value of f_{CO_2} should therefore be estimated by calculating f_{CO_2} for a monthly mean value at a consistent SST appropriate to the gas flux calculation. As explained in detail below, we use a representative, accurate and consistent value of SST for each grid-cell value of f_{CO_2}.

The focus of this paper is to critically assess f_{CO_2} calculations and the application of f_{CO_2} for CO_2 ocean gas flux climatology development, with an emphasis on the need to properly address inconsistencies in SST measurement methods. In other respects, we use simple approaches to the calculation of a climatology (for example, simple geospatial interpolation). We first review the importance of SST to the calculation of f_{CO_2} and the use of satellite SST data. We then review the monthly composite SST data that we derived from SOCAT's regional synthesis files and compare those to satellite observations of SST. In Sect. 2 we briefly describe the SOCAT data set and methods, followed by an explanation of our approach to compute a climatological f_{CO_2} from the SOCAT in situ f_{CO_2} data (Sect. 3). In Sect. 4 the spatial interpolation using ordinary block kriging is detailed and in Sect. 5 the resulting f_{CO_2} climatology and a range of possible errors are discussed. Our application of the recently released SOCAT "version 2" data set is the subject of Sect. 6. The month January is used as an illustrative example of the data treatment throughout this paper. In the conclusion (Sect. 7) SOCAT version 1.5 and 2 and their uses are compared and a recommendation for future versions of SOCAT is given.

In this paper, we explain the reasons for our conversion of f_{CO_2} for in situ SST to f_{CO_2} for monthly composite SST from satellites and the methodology of our conversion in detail. The resulting data sets are useful for air–sea gas flux studies and are given as a supplement to this publication. We will not interpret the oceanographic features that can or cannot be distinguished in our maps. We leave that to continuing work within and beyond the OceanFlux-GHG project.

1.2 Complexities of in situ SST measurements and implications for f_{CO_2}

As already discussed, f_{CO_2} is highly sensitive to temperature. Similarly, accurate knowledge of SST and, to a lesser extent, salinity, is essential when calculating air–sea gas fluxes. SST vertical profiles are complex and variable. SST can also vary over relatively short time scales within relatively small regions and variations in the temperature measured can also arise from the method and instrumentation used for measur-

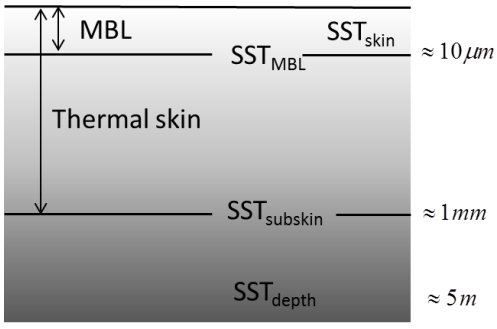

Figure 1. A schematic of the surface ocean, depicting the definition of the mass boundary layer (MBL), thermal skin and temperatures at various depths (Donlon et al., 2002). SST_{depth} can be from centimetres to metres below the surface, but is commonly around 5 m in the SOCAT data.

ing it. All of these issues can cause problems when using in situ data to construct a f_{CO_2} climatology. These issues are now discussed. We begin with issues surrounding individual measurements of SST and then consider the quality of composite values of in situ derived SST (i.e. averages over a defined grid cell).

The structure of the upper ocean (~ 10 m) vertical temperature profile depends on the level of shear-driven ocean turbulence and the air–sea fluxes of heat, moisture and momentum. Every SST observation depends on the measurement technique and sensor that is used, the vertical position of the measurement within the water column, the local history of all components of the heat flux conditions and, the time of day the measurement was obtained (Donlon et al., 2002). The subsurface SST, SST_{depth} (Fig. 1), will encompass any temperature within the water column where turbulent heat transfer processes dominate (Donlon et al., 2007). Such a measurement may be significantly influenced by local solar heating, the variations of which have a time scale of hours, and typically temperature will vary with depth. Diurnal warming and the formation of a "warm layer" may occur at the sea surface when incoming shortwave radiation leads to stratification of the surface water. In the absence of wind-induced mixing, temperature differences of > 3 K can occur across the surface warm layer (Ward et al., 2004), which in turn will enhance the outgassing flux of CO_2 (Jeffrey et al., 2007, 2008; Kettle et al., 2009). In order to address such issues, the international Group on High Resolution Sea Surface Temperature (GHRSST) states that SST_{depth} should always be quoted at a specific depth in the water column; for example, $SST_{5\,m}$ refers to the SST at a depth of 5 m. However, SST_{depth} data can be measured using a variety of different temperature sensors mounted on buoys, profilers and ships at any depth beneath the water skin and the depth of the measurement is often not recorded. Different measurement systems that are used to measure SST (e.g. hull mounted thermistors, inboard thermosalinograph systems) have evolved over time using different techniques that are prone to different error characteristics (e.g. for a good review see Kennedy, 2013; Kennedy et al., 2011a, b), such as warming of water as it passes through the ships' internal pipes before reaching an inboard thermosalinograph (e.g. Kent et al., 1993; Emery et al., 2001; Reynolds et al., 2010; Kennedy, 2013), poor calibration or biases due to the location and warming of hull mounted temperature sensors (e.g. Emery et al., 1997, 2001), inadequate knowledge of temperature sensor depth (e.g. Emery et al., 1997; Donlon et al., 2007), poor knowledge of temperature sensor calibration performance and local thermal stratification during a diurnal cycle (e.g. Kawai and Wada, 2007). This means that if not carefully controlled, SST biases of > 1 K may easily be introduced into an in situ SST data set.

An additional set of issues surrounds the calculation of gridded values of SST derived from in situ data. Here, in addition to potential biases in individual measurements, we should consider whether the sampling by in situ methods is sufficient. In respect to the SST measurements paired to CO_2 measurements, there is an issue (Takahashi et al., 2009), which is likely to result from a combination of undersampling, temperature gradients and measurement bias.

All of these issues mean that directly using SST and f_{CO_2} measurement pairs from a large data set (i.e. that resulting from a large number of different instrument set-ups and methods) for a f_{CO_2} climatology for studying air–sea gas fluxes is likely to introduce errors. In summary, three steps must be achieved to estimate true monthly mean values of f_{CO_2} to (1) adjust for errors due to the vertical SST gradient, (2) minimise the bias due to undersampling (related to grid-box averaging of the measurement data), and (3) minimise errors due to the different methods and instrumentation. Therefore, we propose that correcting all of the f_{CO_2} data back to a consistent surface SST data set is clearly advantageous, and this is where satellite data can be useful.

1.3 The use of satellite sea surface temperature data

Satellite Earth observation thermal infrared radiometers have been in orbit around the Earth since the 1990s and global SST products based on these instruments are available. The radiometers are sensitive to thermal radiation from the "radiometric skin" of the ocean and more recent products are calibrated exclusively against other "skin SST" measurements (rather than SST measurements at depth). In addition to individual measurements, composite or gridded values of SST are calculated and these have a low sampling uncertainty for monthly values. These satellite products have been shown to have a higher accuracy and precision for studying SST than in situ methods (e.g. O'Carroll et al., 2008) and such data are now available as a climate data record (Merchant et al., 2008, 2012). We used satellite derived SST values from the Along Track Scanning Radiometers, ATSRs, Reprocessing for Climate project, ARC (Merchant et al., 2012). This climate data

record is a global, long-term, homogenous, highly stable SST data set based on satellite-derived SST observations.

We have mentioned thermal gradients within the upper metres of the ocean, and particularly warm layers, in the previous section, but it is also important to note that the very surface of the ocean and the radiometric skin are typically one to two tenths of a Kelvin cooler than the water millimetres below, due to cooling at the sea surface and limited eddy transport within the top millimetre of the ocean. Thus, a thermal skin is defined as shown schematically in Fig. 1. The low eddy transport also affects gas transport and a mass boundary layer, MBL (Fig. 1), is defined for air–sea gas exchange. Though both the thermal skin and MBL are products of limited eddy transport, MBL is thinner than the thermal skin due to the lower molecular diffusivity of dissolved gases. The concentration difference across MBL is the driving force behind the air–sea flux of CO_2. A calculation of the concentration difference requires attention to vertical thermal gradients both in the top millimetre and in the several metres below. As discussed previously, in situ subsurface seawater fugacity is normally measured several metres below the surface. The direct application of these measurements for deriving air–sea fluxes (e.g. Takahashi et al., 2009) implicitly assumes that the measured fugacity values at depth are the same as those at the bottom of the MBL. The formation of warm layers will certainly undermine this assumption and the thermal skin adds a significant additional complication. Satellites directly provide a radiometric temperature virtually equivalent to the temperature at the top of the thermal skin and MBL. At wind speeds of approximately $6\,\mathrm{m\,s^{-1}}$ and above, the relationship between $\mathrm{SST_{skin}}$ (at the top of the skin) and $\mathrm{SST_{subskin}}$ (Fig. 1) is well characterised for both day- and night-time conditions by a cool bias (e.g. Donlon et al., 2002). Therefore a skin temperature value from Earth observation with an appropriate correction for the cool skin bias can be used to describe the temperature at the base of the thermal skin, thus avoiding the effects of warm layers and other thermal gradients below the skin. Temperatures within the thermal skin (for example, defined for the base of the MBL) are not a standard product, but could also be estimated from $\mathrm{SST_{skin}}$. There are some remaining ambiguities regarding precisely which satellite-based temperature product is optimal for generating a climatology, but any temperature calculated from composite satellite derived SSTs is preferable (to calculate composite values of CO_2 parameters at the base of the MBL) in comparison to an in situ $\mathrm{SST_{depth}}$ product. The practical differences between satellite and in situ temperature products are described in the next section.

1.4 A comparison between SST data sets

In air–sea gas flux calculations, an estimate of the water side f_{CO_2}, and hence the temperature, is required at the base of the mass boundary layer. However, ARC SST data are measurements of the sea surface skin, $\mathrm{SST_{skin}}$, which is characteristically cooler than the water just below it. Since gas transfer velocities are low in low wind speeds, it is more important to have a reasonably accurate estimate of the thermal skin effect in moderate and high wind speeds. Donlon et al. (1999) reported a mean cool skin $\Delta T = 0.14\,(\pm 0.1)$ K for wind speeds in excess of $6\,\mathrm{m\,s^{-1}}$ and so we used this to derive $\mathrm{SST_{subskin}}$ (the SST at the base of the thermal boundary layer, Fig. 1) from ARC $\mathrm{SST_{skin}}$.

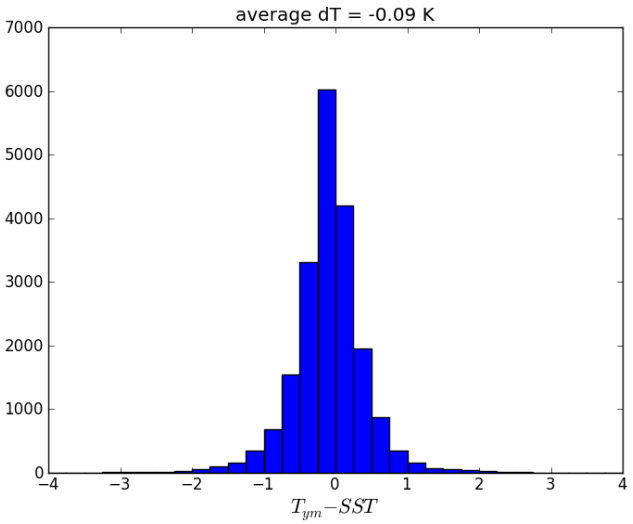

Figure 2. Histogram of temperature difference (K) between monthly gridded data of subskin SST derived from ARC, T_{ym}, and in situ SST from SOCAT version 1.5 using global data from August 1991 to 31 December 2007. The bin widths are 0.25 K, and the average and median dT are both -0.09 K.

The ARC data set provides daily day-time and night-time averages of $\mathrm{SST_{skin}}$ (K) from infrared imagery gridded to a 0.1° latitude–longitude resolution (Merchant et al., 2012). For each year from 01 August 1991 to 31 December 2010, we calculated the monthly mean $\mathrm{SST_{skin}}$ distributions, averaged over a $1^\circ \times 1^\circ$ grid without differentiating between day- and night-time measurements (http://www.oceanflux-ghg.org/Products/OceanFlux-data/Monthly-composite-datasets). These $\mathrm{SST_{skin}}$ grid points were linearly interpolated to the ith SOCAT measurement location ($\mathrm{SST_{skin},}_i$). We defined T_{ym} (K) as the $1^\circ \times 1^\circ$ grid box mean of $T_{\mathrm{ym},i} = \mathrm{SST_{skin},}_i + 0.14\,\mathrm{K}$ in the measurement year "y" and measurement month "m". The f_{CO_2} values were then re-computed from in situ SST to satellite $T_{\mathrm{ym},i}$ for our climatology (Sect. 3.2).

Using $1^\circ \times 1^\circ$ grid box means of the difference between $T_{\mathrm{ym},i}$ and SOCAT's instantaneous in situ SST measurement (generally obtained at 5 m nominal depth) converted to unit K and all data from the years 1991 to 2007, a histogram of $\mathrm{d}T = T_{\mathrm{ym}} - \mathrm{SST}$ (K) was produced (Fig. 2). It shows that dT was distributed around a median and mean of -0.09 K with a standard deviation of 0.55 K. Assuming the cool skin effect has been corrected accurately, this difference implies

that the gridded in situ SST systematically overestimated T_{ym} (our estimate of $SST_{subskin}$). The corresponding histogram of $1° \times 1°$ grid box means of the difference between f_{CO_2} converted to a monthly composite and the original SOCAT's in situ f_{CO_2} ($df_{CO_2} = f_{CO_2}(T_{ym}) - f_{CO_2}$) using data from all years (not shown) revealed a similar distribution with a mean of -1.21 µatm and standard deviation of 9.36 µatm. The temperature differences were found to be positive as well as negative (Fig. 2). Positive dT can be a consequence of diurnal warming when the top layer heats up by solar radiation during the day. This heat is lost again during the night. Cooling of the top layer (negative dT) is a less described phenomenon but can be expected in colder environments. Alternatively, it is possible that negative dT results because the in situ data are biased warm, perhaps because the warming before reaching a ship-board thermosalinograph is systematically underestimated. We found more negative dT during the winter months and at high latitudes. The temperature profile in the sea depends on wind speed as wind mixes the water column, i.e. for strong winds SST is expected to be more constant in the vertical. Figure 3 illustrates the wind speed dependence of dT for the North Atlantic. This region was chosen because it has the highest SOCAT data density. For each dT we retrieved the monthly $1° \times 1°$ grid box mean of 10 m wind speed, U_{10} ($m\,s^{-1}$), using the Oceanflux-GHG's composite of GlobWave merged altimeter wind speed data (http://www.oceanflux-ghg.org/Products/OceanFlux-data/Monthly-composite-datasets). The scatter plot of dT as a function of U_{10}, averaged over in $1\,m\,s^{-1}$ U_{10} bins, (Fig. 3) shows that dT decreased with increasing U_{10} becoming negative for wind speeds over about $10\,m\,s^{-1}$. Similar trends were seen in the other regions, but with dT turning negative for different wind speeds: North Pacific $9\,m\,s^{-1}$; Coastal $8\,m\,s^{-1}$; Tropical Atlantic and Southern Ocean $6\,m\,s^{-1}$; Tropical Pacific, Indian Ocean and Arctic $4\,m\,s^{-1}$. The Tropical Atlantic was different in that dT became less negative for wind speed over $\sim 8\,m\,s^{-1}$, turning positive over $\sim 10\,m\,s^{-1}$. If only North Atlantic data from the winter months December, January and February were included, nearly all dT values were negative. The analyses of SST differences described above, suggest strongly that the original in situ temperatures are biased and that bias varies spatially and seasonally. Therefore, a correction of CO_2 parameters for temperature is appropriate.

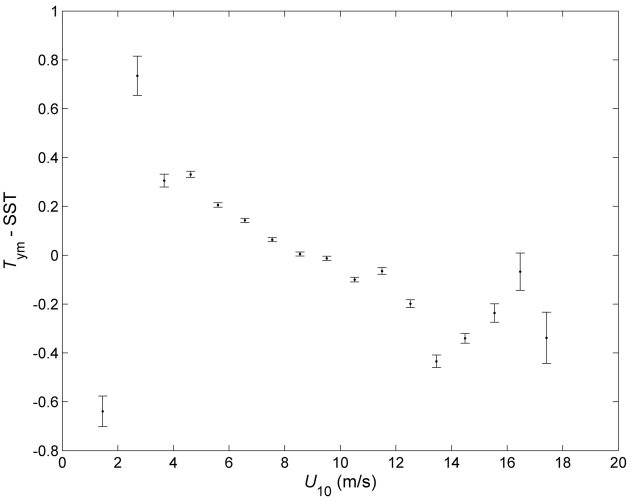

Figure 3. Scatter plot of temperature difference (K) between monthly gridded data of subskin SST derived from ARC, T_{ym}, and in situ SST from SOCAT version 1.5, using data from all available years in the North Atlantic, binned in $1\,m\,s^{-1}$ U_{10} bins. The error bar indicates the standard error of the mean.

1.5 Corrections of f_{CO_2} for SST

Having concluded that the temperature originally paired with a CO_2 measurement is not suitable for a gridded air–sea flux calculation, we require a guiding principle to calculate "revised values" that can be paired with consistent and appropriate SST values throughout the flux calculations. The principle that we apply is that for changes in temperature within each grid cell, the fugacity changes can be calculated to a good approximation by assuming the changes in the carbonate system are isochemical. That principle is standard for corrections within a measurement system (for example where the sample water is warmed between collection and measurement in an equilibrator) and can also be applied with some confidence to the changes effected by warm layer formation and destruction (Olsen et al., 2004; Jeffery et al., 2007). Applying the principle more broadly is less satisfactory, but given the value of calculating consistent and robust values of temperature and carbonate parameters for air–sea flux calculations, it is a reasonable action. Essentially, we assume that there will not be systematic sample biases in alkalinity or total dissolved inorganic carbon within the grid cell, but the original temperatures may be poorly measured, poorly sampled or affected by vertical temperature gradients. Dissolved inorganic carbon is partitioned between dissolved gas, bicarbonate ions and carbonate ions and the fractions of each is temperature dependent. An isochemical change in the system changes the concentration and fugacity of the dissolved gas without altering the alkalinity or the total dissolved inorganic carbon. In Sect. 3, we describe the recalculation of fugacities and partial pressures by applying this principle.

An important subtlety is that we recalculate fugacity at $SST_{subskin}$ rather than the theoretical temperature at the base of MBL. Some of the reasons are simply pragmatic: e.g. calculating $SST_{subskin}$ is quite standard and the correction to composite values of this temperature achieves the primary objective, since the temperature difference with in situ temperatures (Figs. 2 and 3) is generally larger than those within the thermal skin. Another reason is theoretical: the response time of the carbonate system is limited by the hydration reaction and it is unlikely that substantial repartitioning (and changes in the concentration of the dissolved gas) will oc-

cur between the base of the thermal skin and the base of the MBL. Therefore a concentration calculated from the solubility and fugacity at $SST_{subskin}$ should also be appropriate for the base of the MBL.

An overview of all the different parameters used in our re-computation is presented in Appendix A1. The SOCAT measurements and methods are described in Sect. 2 and Appendix A2 and our re-computation in Sect. 3 and Appendix A3.

2 The SOCAT measurements

2.1 The SOCAT database

The SOCAT database contains millions of surface-ocean CO_2 measurements in all ocean areas spanning four decades (Bakker et al., 2014; Pfeil et al., 2013). All data are put in a uniform format, while clearly defined criteria are applied in their quality control. SOCAT has been made possible through the cooperation (data collection and quality control) of the international marine carbon science community. The history and organisation of SOCAT is described in Pfeil et al. (2013). SOCAT version 1.5 includes 6.3 million measurements from 1968 to 2007 and was made publicly available in September 2011 at http://www.socat.info/SOCATv1/. SOCAT data are available as three types of data products: individual cruise files, gridded products and merged synthesis data files. For our study we used the latter and we downloaded the individual regional synthesis files from http://cdiac.ornl.gov/ftp/oceans/SOCATv1.5/. The content of these files (parameter names, units and descriptions) are described in Table 5 in Pfeil et al. (2013). The data can be displayed in the online Cruise Data Viewer (Fig. 4) and downloaded in text format. More recently, on 04 June 2013, the updated database SOCAT version 2 was released containing 10.1 million surface water f_{CO_2} values (Bakker et al., 2014). Additional data are from cruises during the years 2008 to 2011, from the Arctic, and previously unpublished data from earlier cruises. Also the quality control is tightened and some data has been removed.

2.2 Measurements of p_{CO_2} (T_{eq})

The measurement method of p_{CO_2} in seawater described by Takahashi et al. (2009) is summarised in the following. On board the ship a head space of an equilibrator is equilibrated with streaming seawater and the concentration of CO_2 in the equilibrated carrier gas is measured. When a dry carrier gas is analysed, seawater p_{CO_2} (T_{eq}) in the equilibrator chamber at temperature T_{eq} is computed using

$$p_{CO_2}(T_{eq}) = x_{CO_2,dry}(P_{eq} - P_w) \quad (1)$$

where P_{eq} is the pressure at the equilibrator (atm), P_w water vapour pressure (atm) at T_{eq} and salinity (S), and $x_{CO_2,dry}$ the mole fraction of CO_2 in dry air (ppm) for p_{CO_2} in µatm. P_w (atm) is calculated with

$$P_w = \exp(\,24.4543 - 67.4509(100/T_{eq}) - 4.8489\ln(T_{eq}/100) - 0.000544S\,) \quad (2)$$

with T_{eq} in K (Pfeil et al., 2013). When mixing ratios in a wet carrier gas (100 % humidity) are determined, P_w is absent

$$p_{CO_2}(T_{eq}) = x_{CO_2,wet} P_{eq} \quad (3)$$

2.3 Temperature handling

There are different methods to correct for the difference in partial pressure at intake and equilibrator temperature. SOCAT uses the simple Eq. (A1) (Pfeil et al., 2013). Takahashi et al. (2009) note that a more complicated formula

$$p_{CO_2,is} = p_{CO_2}(T_{eq})\exp(\,0.0433(SST - T_{eq}) - 4.35\times10^{-5}(SST^2 - T_{eq}^2)\,) \quad (4)$$

is more accurate, with SST and T_{eq} in °C. Equations (A1) and (4) correct for the effect of slight warming before measurement at the equilibrator in an isochemical transformation. Equation (4) is an integrated form of

$$\delta\ln(p_{CO_2})/\delta T = 0.0433 - 8.7\times10^{-5}T,$$

with temperature, T (°C), while in Eq. (A1) a constant coefficient of $0.0423\,°C^{-1}$ is used. Equation (4) should be slightly more accurate, but it can be shown that the simpler form will not be a major source of bias in $p_{CO_2,is}$ estimates.

3 Our re-computation for climatological fugacity in the year 2010

In our re-computation of f_{CO_2} for SOCAT's in situ SST to monthly composite f_{CO_2} we only used "good" records (WOCE_flag = 2) with valid $f_{CO_2,is}$ and SST. Our re-computation required multiple steps (see Appendix A1 for definitions of variables):

1. estimate original p_{CO_2} measurement at T_{eq};
2. convert $p_{CO_2}(T_{eq})$ to $p_{CO_2}(T_{ym,i})$;
3. calculate $f_{CO_2}(T_{ym,i})$ from $p_{CO_2}(T_{ym,i})$;
4. apply linear trend to extrapolate $f_{CO_2}(T_{ym,i})$ and $p_{CO_2}(T_{ym,i})$ to year 2010;
5. bin the data by month and in 1° × 1° grid boxes;
6. spatially interpolate the grid boxes.

The first three steps were necessary because mole fraction $x_{CO_2,is}$, and partial pressures $p_{CO_2,is}$ and $p_{CO_2}(T_{eq})$ are not given in the SOCAT regional synthesis files (so Eqs. A2 and

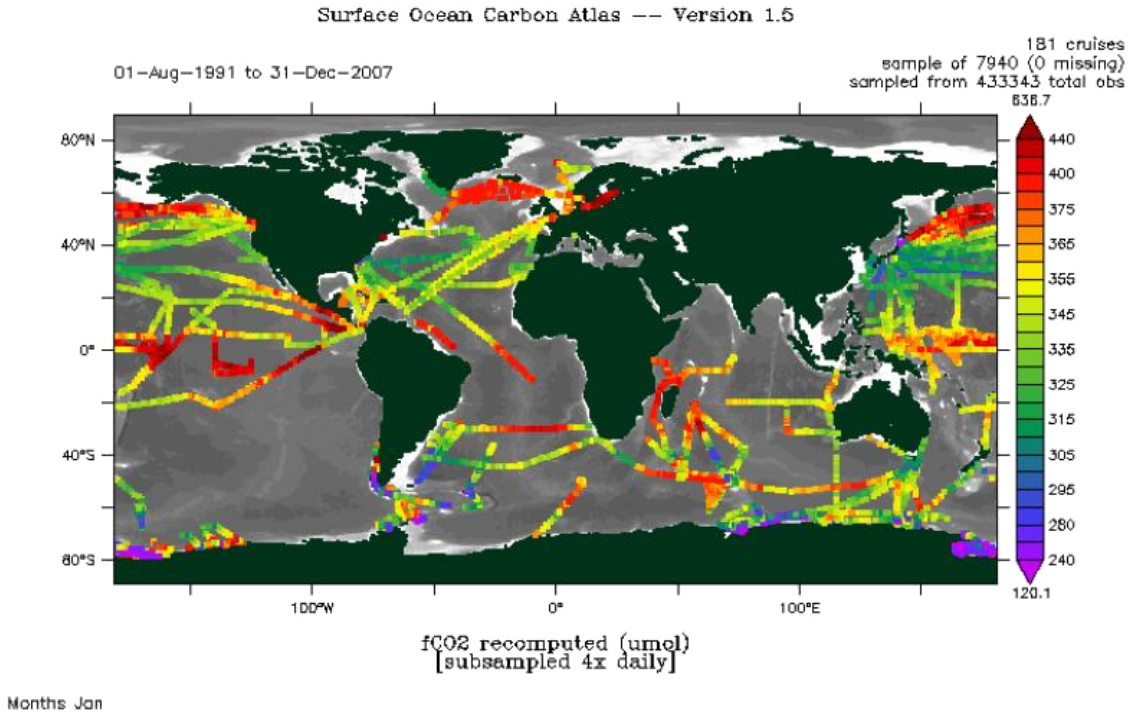

Figure 4. SOCAT version 1.5 CO_2 fugacity (µatm) data shown in the online Cruise Data Viewer at http://www.socat.info/ for the month January from 1992 to 2007.

4 could not be used directly to calculate $f_{CO_2,ym,i}$). The first step of estimating the original measurement of $p_{CO_2}(T_{eq})$ is described in Appendix A3. Note also that by first returning to the partial pressure at the equilibrator temperature, any measurement bias in the in situ temperature is removed thereafter. If T_{eq} was not given we skipped step 1 and used SST to convert p_{CO_2}(SST) to $p_{CO_2,ym,i}$ in step 2; those records will carry the effect of any measurement bias in the in situ temperature into the recalculated values. The next step was to convert partial pressure at equilibrator temperature to partial pressure at $T_{ym,i}$ for each SOCAT measurement. Because ARC ATSR data were available from 01 August 1991 we converted SOCAT data from 01 August 1991 until 31 December 2007. As a consequence 95249 (1.4 %) of valid f_{CO_2} observations were not used from the SOCAT v1.5 data set (from 119 cruises spread all over the globe). We note that the ESA SST Climate Change Initiative (CCI) project is now working on an extended SST climate data record from satellite extending back to 1981, which is expected to be made available in 2015. We used Eq. (4) to correct for the difference between monthly composite and equilibrator temperature in °C resulting in

$$p_{CO_2,ym,i} = p_{CO_2}(T_{eq}) \exp \left(0.0433(T_{ym,i} - T_{eq}) - 4.35 \times 10^{-5}(T_{ym,i}^2 - T_{eq}^2)\right) \quad (5)$$

The subscript "ym" indicates a "single year monthly composite" and "i" interpolated to SOCAT sample location (Sect. 1.4). As explained in Sect. 1.5, Eq. (4) was applied on the basis that an isochemical transformation between SST and T_{ym} is a reasonable assumption. In a third step, monthly composite estimations of $f_{CO_2,ym,i}$ (µatm) were calculated from $p_{CO_2,ym,i}$ by inverting Eq. (A2),

$$f_{CO_2,ym,i} = p_{CO_2,ym,i} \exp \left(\frac{\left[B + 2\left(1 - \frac{p_{CO_2}(T_{eq})}{P_{eq,ym}}\right)^2 \delta \right] P_{eq,ym}}{R \cdot T_{ym,i}} \right) \quad (6)$$

with $B = B$ (CO_2, $T_{ym,i}$) (Eq. A3) and $\delta = \delta$ (CO_2, $T_{ym,i}$) (Eq. A4) and temperatures in K. We estimated $P_{eq,ym}$ from sea level pressure estimated at closest grid value from 6 hourly NCEP/NCAR as given in SOCAT's merged synthesis files (ncep_slp in hPa). To account for the overpressure that is normally maintained inside a ship 3 hPa was added ($P_{eq,ym}$ = ncep_slp + 3 hPa) (Takahashi et al., 2009) and $P_{eq,ym}$ was converted to unit atm. Note that we recomputed SOCAT's f_{CO_2} for monthly composite SST and atmospheric pressure, but not for monthly composite salinity. However, if in situ salinity was not provided by the investigator, SOCAT used a monthly composite sea surface salinity from the World Ocean Atlas 2005 (woa_sss) for their computation of $f_{CO_2,is}$. The consequences of absent salinity values are assessed in Sect. 5.7. For all years $p_{CO_2,ym,i}$ and $f_{CO_2,ym,i}$ were extrapolated to the year 2010, produc-

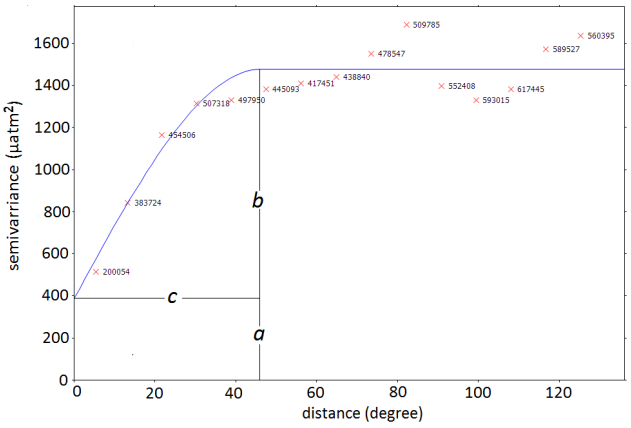

Figure 5. Variogram for global $f_{CO_2,cl}$ data in 2010 for the month January, derived from $f_{CO_2,is}$ shown in Fig. 4. The numbers next to each data point are the number of data pairs.

ing $p_{CO_2,cl,i}$ and $f_{CO_2,cl,i}$ referenced to 2010, using the same mean rate of change (1.5 ± 0.3 µatm y^{-1}) as Takahashi et al. (2009) used for p_{CO_2}. The Takahashi et al. (2009) study extrapolated to the year 2000 only, so if the rate of change has increased since then, our estimates for 2010 could be biased low. Finally, the $f_{CO_2,cl,i}$ and $p_{CO_2,cl,i}$ data were grouped by month and averaged over $1° \times 1°$ squares. Not all $1° \times 1°$ grid boxes were filled and we horizontally interpolated between filled values to produce global $p_{CO_2,cl}$ and $f_{CO_2,cl}$ distributions (Sect. 4).

4 Horizontal extrapolation using ordinary block kriging

Unlike Takahashi et al. (2009), our climatology includes data from El Niño years and coastal locations. We added $p_{CO_2,cl}$ for those who prefer to use partial pressure; $p_{CO_2,cl}$ levels were slightly higher (less than 2 µatm) than $f_{CO_2,cl}$. For the spatial interpolation of the gridded data on a $1° \times 1°$ mask map of the global oceans, we used the variograms and kriging options within gstat, which is an open source tool for multivariable geostatistical modelling, prediction and simulation (gstat home page: http://www.gstat.org/). Gstat finds the best linear unbiased prediction (the expected value) with its prediction error for a variable at a location, given observations and a model for their spatial variation (Pebesma, 1999, 2004). We used the "ordinary block kriging" option. We quantified the prediction error as standard deviation, SD (square root of the variance given by gstat). As would be expected, the prediction errors were large in areas with data sparsity. First, we modelled the variogram for $f_{CO_2,cl}$ for each month using gstat's interactive user interface (Pebesma, 1999, 2004). A variogram describes how the data vary spatially and can be represented by a plot of semivariance against distance. The variograms best fitted combinations of a nugget and a spherical model, a Nug$(0) + b$ Sph(c), and for each month variogram parameters a, b and c were derived (e.g. Fig. 5). Figure 5 shows that at small separation distances, the semivariance in f_{CO_2} (computed as one-half of the difference in f_{CO_2} squared) is small, so that points that are close together have similar f_{CO_2} values. After a certain level of separation (c), the variance in the f_{CO_2} values becomes rather random and the model variogram flattens out to a value corresponding to the average semivariance ($a + b$). The model variogram is used to compute the weights used in the kriging. The variogram coefficients were different for each month because each monthly data set had a different data distribution. The fitted variogram models were applied in the kriging of both $f_{CO_2,cl}$ and $p_{CO_2,cl}$ because the difference with $f_{CO_2,cl}$ was negligible compared to the spatial variation. By using the variogram to compute the weights for the interpolation, the expected estimation error is minimised in a least squares sense so that the kriging produces the best linear unbiased estimate.

We applied ordinary kriging on mask map locations because it is the default action when observations, variogram, and prediction locations are specified (Pebesma, 1999). We performed local ordinary block kriging directly on a $1° \times 1°$ mask map of the global oceans with minimum (min) of 4, maximum (max) of 20, and radius of 60°. Thus, after selecting all data points at (euclidian) distances from the prediction location less or equal to 60°, the 20 closest were chosen when more than 20 were found and a missing value was generated if less than 4 points were found. It should be noted that the interpolation did not necessarily stop at land barriers in areas with few or no data points. Also the decorrelation length was most likely shorter than 60° kriging radius for the majority of the grid cells (Jones et al., 2012). Jones et al. (2012) do not show that changes in surface-ocean p_{CO_2} are larger in either the east–west direction or the north–south direction. We had to choose between a small kriging radius and generating a few high-quality grid cells but many empty grid cells, or a large kriging radius and generating few empty grid cell values but many with high SDs. We chose the latter in order to produce almost complete maps and with the option that a quality filter could be applied later. The data were smoothed by averaging over square shaped $5° \times 5°$ sized blocks. Thus gstat produced the $f_{CO_2,cl}$ (and $p_{CO_2,cl}$) prediction and variance values located at the grid cell centres of the (non-missing valued) cells in the grid map mask. These results were compared with results from different kriging options min, max, radius and block size (Sect. 5.3).

Our approach to the interpolation of these sparse data is simpler and more straightforward than other previous methods. This choice was deliberate as optimal interpolation of such sparse environmental data is itself a focus of international research. For example, the spatial interpolation on a $4° \times 5°$ grid of Takahashi et al. (2009) applies a knowledge of ocean circulation. Available observations were first propagated to neighbouring pixels with no observations by in-

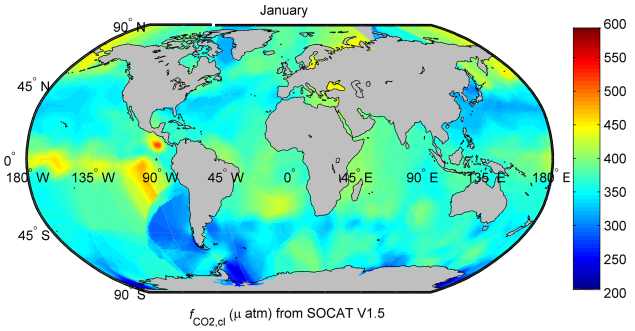

Figure 6. Monthly $f_{CO_2,cl}$ values (µatm) in the global oceans estimated for January 2010 on a 200–600 µatm scale; data were interpolated to a $1° \times 1°$ grid using ordinary block kriging with min = 4, max = 20, radius = 60° and block size $5° \times 5°$.

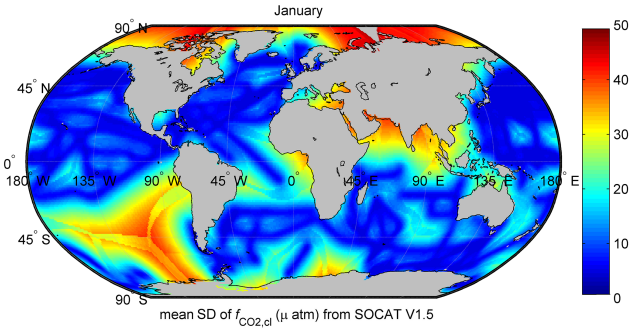

Figure 7. Standard deviation in $f_{CO_2,cl}$ (µatm) estimated for January 2010 on a 0–50 µatm scale, associated with the ordinary block kriging shown in Fig. 6.

cluding the values in neighbouring areas for ±4° latitude, ±5° longitude and ±1 day from the center of a pixel. The values of the pixels that are still without observations after this procedure are computed by a continuity equation based on a 2-D diffusion–advection transport equation for surface waters. All daily pixel values are used to calculate monthly mean values. Takahashi et al. (2009) estimate that the global mean surface water $p_{CO_2,cl}$ obtained in their study may be biased by about +1.3 µatm due to under sampling and their interpolation method. Our use of a consistent and unbiased temperature for f_{CO_2} calculations should reduce this bias. Further examples of more advanced interpolation schemes include: Landschützer et al. (2013) who applied a two-step neural network to interpolate SOCAT observations in space and time and derive basin-wide monthly maps of p_{CO_2} on a $1° \times 1°$ grid. The neural networks fit the observations with almost no bias. Rödenbeck et al. (2013) used a model of surface-ocean biogeochemistry to temporally and spatially resolve (with respective resolutions of 1 day and $4° \times 5°$) global surface-ocean p_{CO_2} from the SOCAT's f_{CO_2} database and Park et al. (2010) construct monthly climatological maps of p_{CO_2} on a global $4° \times 5°$ grid using sub-annual $\delta p_{CO_2}/\delta$ SST trends and inter-annual SST anomalies.

5 Results

5.1 Monthly global maps

The prediction distributions of $f_{CO_2,cl}$ produced by the ordinary block kriging are shown in Fig. 6 for January; Fig. 7 shows the associated standard deviations and Fig. 8 the $f_{CO_2,cl}$ predictions with high prediction errors (SD > 25 µatm) masked. Grid-box values, as shown in Fig. 8 for January, were averaged over 3 months (an empty grid box was generated if it did not contain at least one valid value with SD < 25 µatm) resulting in four seasonal distributions of $f_{CO_2,cl}$ (Fig. 9). The 12-monthly global distribution data have been made available in 12 NetCDF files in the supplement related to this article. These files contain $f_{CO_2,cl}$, $p_{CO_2,cl}$, their kriging errors, and ARC's SST_{skin} for the year 2010, all on a $1° \times 1°$ grid. The variable names are respectively fCO2_2010_krig_pred, pCO2_2010_krig_pred, fCO2_2010_krig_std, pCO2_2010_krig_std, and Tcl_2010 (T_{ym} as defined in Sect. 1.4 for the year 2010). Also given is vCO2_2010, the mole fraction of CO_2 in dry air (ppm) in 2010 from the Earth System Research Laboratory of the National Oceanic and Atmospheric Administration, NOAA ESRL, (Dlugokencky et al., 2014) on the $1° \times 1°$ grid. This variable is not used in our re-computation, but is included because it is used in air–sea flux calculations. The important differences with the Takahashi climatology are summarised in Table 1.

A comparison between the Takahashi climatology, normalised to the year 2010 by adding 15 µatm ($= 1.5\,\mu atm\,yr^{-1} \times 10\,y$), and OceanFlux $p_{CO_2,cl}$ is shown in Fig. 10. The general distribution is similar with large differences mainly confined to poorly sampled regions such as the Arctic and some coastal zones. For the well-sampled zone 14–50° N in the North Atlantic and North Pacific, the climatologies are satisfactorily similar, with the discrepancies of the respective seasonal $p_{CO_2,cl}$ averages being less than ∼2.4 and ∼4.4 µatm (Table 2), but there are some interesting if subtle differences. For instance, both products exhibit a seasonal signal in the North Atlantic but the amplitude of that seasonal signal is noticeably stronger in the new product (thus positive difference in summer, negative difference in the winter).

Differences with Takahashi and other climatologies arise for four key reasons.

1. The selection of data. Our product relies on quality control within SOCAT and should in this respect be comparable to other products derived from SOCAT, but may differ significantly from Takahashi et al. (2009) for which the selection of data is less transparent.

Table 1. Comparison between Takahashi climatology and climatology presented in this paper (both using trend of 1.5 µatm yr^{-1}).

	Takahashi et al. (2009)	This study
Data source	LDEO database (NDP-088) http://cdiac.ornl.gov/oceans/doc.html (Takahashi et al., 2009)	SOCAT versions 1.5 and 2 (synthesis data files) http://www.socat.info/ (Pfeil et al., 2013; Bakker et al., 2014)
Period covered	1970–2007	01 August 1991–31 December 2007/11 (SOCAT v1.5/2)
Reference year	2000	2010
Resolution	$4^\circ \times 5^\circ$ and 1month	$1^\circ \times 1^\circ$ and 1 month
Data	Excludes El Niño periods in the equatorial Pacific and coastal data	Includes El Niño and coastal data
Spatial interpolation	Involves continuity equation based on a 2-D diffusion–advection transport equation for surface waters	Ordinary block kriging (without continuity equation)
Parameter	p_{CO_2} (µatm)	f_{CO_2} (and p_{CO_2}) (µatm)
Trend	$+1.5$ µatm yr^{-1}	$+1.5$ µatm yr^{-1}
f_{CO_2} taken at	Instantaneous intake temperature SST_{depth}	Monthly composite sub-skin SST from ARC

Table 2. Seasonal averages in µatm of OceanFlux $p_{CO_2,cl}$ and $p_{CO_2,cl}$ from Takahashi (2009) normalised to 2010 by adding 15 µatm ($= 1.5$ µatm $yr^{-1} \times 10$ yr) in the North Atlantic and North Pacific in the zone 14–50° N.

Ocean basin	Method	Winter	Spring	Summer	Autumn
Atlantic (14–50° N)	OceanFlux	356.8	356.6	382.0	374.7
	Takahashi	358.2	356.9	379.5	372.6
	Difference	−1.4	−0.3	2.5	2.1
Pacific (14–50° N)	OceanFlux	348.8	351.8	379.3	365.6
	Takahashi	353.2	354.8	375.6	369.1
	Difference	−4.4	−3.0	3.7	−3.5

2. The handling of temperature. Our methods differ substantially from those used previously. As explained earlier, we are convinced our handling is more rational and consistent with the eventual calculation of fluxes. Though the mean difference in temperature is fairly small, we have noted already that some regional and seasonal differences are large.

3. The interpolation methods. We have deliberately used a very simple interpolation method based on block kriging. As shown by Figs. 7 and A4, the resulting standard deviations are large and the appearance in poorly sampled regions and seasons is poor. These sparsely sampled regions are not the only regions that show some very obvious differences with Takahashi, for example the eastern-central equatorial Pacific. Other methods produce superficially more pleasing results in the sparsely sampled regions, but they rely on relationships with other variables (e.g. circulation or temperature) that may or may not be robust.

4. The reference year and assumed secular trends. These are clearly significant, but the sensitivity to secular trends in oceanic p_{CO_2} will need to be investigated in a later study.

Calculating all errors is difficult, but we considered the following errors. The prediction errors were estimated by taking the square root of the variances of the kriging. The different kriging approaches themselves were evaluated by calculating the mean and standard deviations of the varying $f_{CO_2,cl}$ kriging results using the options shown in Table 3. The specific timing and path of ship tracks can affect the results. Therefore we used a bootstrapping approach to investigate if certain cruises dominated the mapped results. Other errors that were analysed were the "temporal extrapolation error", the "inversion error" related to the different starting points of the

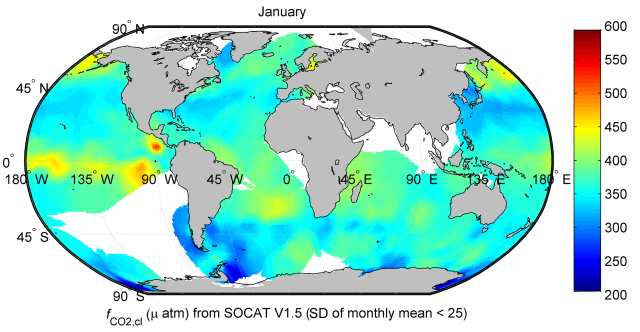

Figure 8. As Fig. 6 but with SD > 25 µatm (Fig. 7) blanked out.

conversion, the consequences of the absent values in our recomputation, and the propagations of the uncertainties in the SOCAT measurements and $T_{\mathrm{ym},i}$. These errors are discussed in the next sub sections and the final subsection gives a summary overview.

5.2 Spatial interpolation errors

The standard deviations (SDs) of the prediction produced by the kriging were calculated by taking the square root of the variance values produced by gstat (Pebesma 1999). These prediction errors were related to the available SOCAT data density in each measurement month (e.g. Figs. 4 and 7) and also to errors in the grid point values of $f_{\mathrm{CO_2,cl}}$ themselves as they are propagated in the kriging operation. For each month we calculated the global mean, min and max of the SD. Over the 12 months, the monthly SD over all grid points was 20 ± 5 µatm on average (mean over all monthly means $\pm$ SD of the mean). The average monthly minimum/maximum SD values were $6.3 \pm 2.6/50 \pm 8.7$ µatm (mean over all monthly min max values $\pm$SD of the mean). Areas with large SD emerged where no SOCAT data were available, for example in the western Southern Ocean and the Arctic. Spatial interpolation errors were lowest in the North Atlantic and North Pacific where SOCAT data was densest. The month April showed the highest errors, this could be a consequence of the variogram range, c, being the smallest, implying that the covariance between the locations dropped quickly with distance In other words, the spatial autocorrelation length was short in April (24°), indicating that $f_{\mathrm{CO_2}}$ was spatially less stable in April (Jones et al., 2012), and the consequent error was recognised by the kriging method. Our variogram model of combination of a nugget and a spherical model did not fit November data satisfactorily as the semivariance was almost independent of distance, meaning that spatial dependence was random, i.e. a near-zero spatial autocorrelation length; thus the low standard deviations in November were therefore probably not representative of the true error due to the kriging method. The low spatial stability in April and November was likely explained by SST or biological activity (or both) being less spatially stable in these months (Jones et al., 2012). Standard deviations of the kriging are included in our presented data files; a bias should not be introduced by the kriging itself (Pebesma, 1999).

Table 3. The different kriging options that were applied to the monthly data sets of $f\mathrm{CO_{cl}}$ for 2010; ordinary block kriging was applied with min, max, radius, dx and dy as explained in Sect. 4.

Min	Max	Radius (°)	dx (°)	dy (°)
4	20	60	5	5
4	20	40	5	5
4	20	100	5	5
4	20	60	1	1
4	20	60	10	10
4	10	60	5	5
4	40	60	5	5
2	20	60	5	5
10	20	60	5	5

5.3 A comparison of the different kriging approaches

The ordinary block kriging of the $f_{\mathrm{CO_2,cl}}$ data was repeated using a range of sensible kriging parameters (Table 3). The standard deviation of the mean over the different kriging results was less than 5 µatm in most places, with higher values seen near the coasts, Arctic, and the western Tropical Pacific and Southern Ocean. These standard deviations were considerably smaller than those of the kriging itself (Figs. 7 and A4) but could be significant in a few places especially, but not exclusively, in the Arctic and coastal regions where the SOCAT data are particularly sparse.

5.4 Are some cruises more important than others?

The specific timing and track of a cruise may give an unrepresentative sample of that region and season. Therefore, it is important to investigate whether or not the final results are highly dependent on individual cruises. That possibility was studied using the bootstrap method, a statistical technique which permits the assessment of variability in an estimate using just the available data (Wilmott et al., 1985). Bootstrapping creates synthetic sets of data by random resampling from the original data with replacement. We bootstrapped the SOCAT data 10 times by cruise to estimate the variability of the mean monthly $f_{\mathrm{CO_2,cl}}$ distributions. Due to the size of the data set we applied the bootstrapping in two stages, first by the cruise's unique identifier (cruise ID) for each year and region, and then by year and region. Each of the 10 resulting synthetic $f_{\mathrm{CO_2,cl}}$ data sets were kriged as described in Sect. 4 (for each month in each synthetic data set the optimal variogram model was fitted and applied). The mean monthly distributions showed that in regions of fewer cruises (i.e. all regions except the North Atlantic and North Pacific) significant variation in $f_{\mathrm{CO_2,cl}}$ could occur; the resulting variations can have a SD of up to 50 µatm. We con-

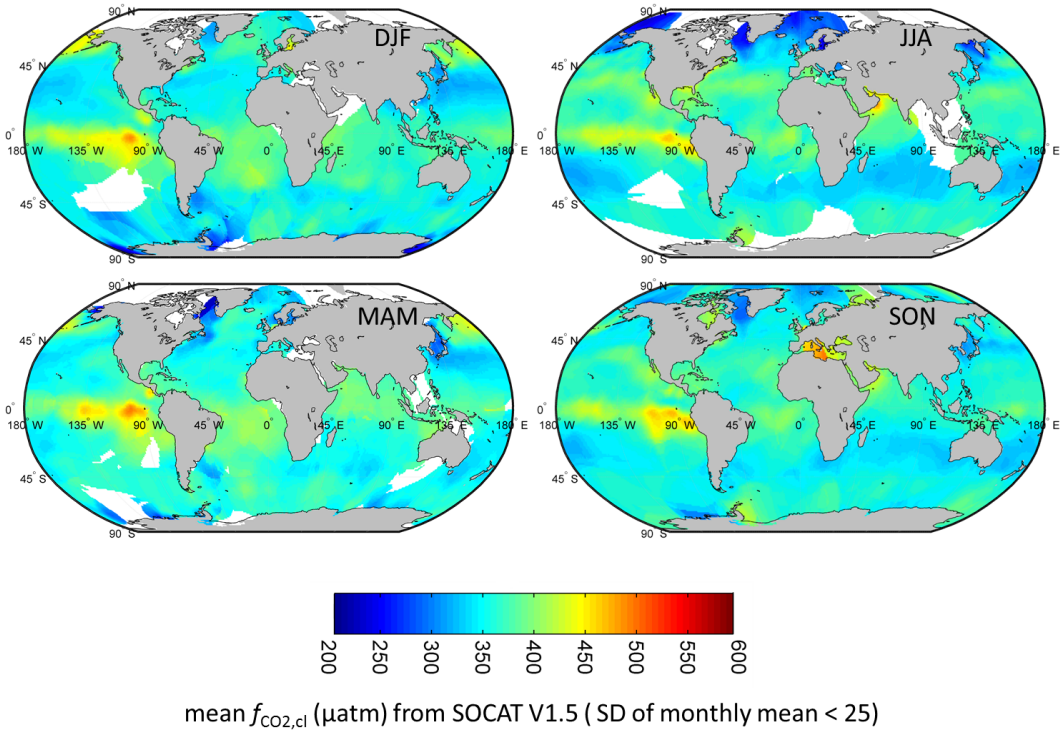

Figure 9. Seasonal $f_{CO_2,cl}$ values (µatm) in the global oceans estimated for 2010 in DJF (December–February), MAM (March–May), JJA (July–August) and SON (September–November) on a 200–600 µatm scale; grid-box values as shown in Fig. 8 for January were averaged over the 3 months.

clude that the final results are highly sensitive to individual cruises in many regions and additional caution in the results should be considered. High variability in the eastern–central equatorial Pacific could be a consequence of not excluding the El Niño years.

5.5 Temporal extrapolation error

The 1.5 µatm yr^{-1} rate of change in p_{CO_2} has an estimated precision of ±0.3 µatm yr^{-1} (Takahashi et al., 2009) and the trend for $f_{CO_2,cl}$ should follow the trend for $p_{CO_2,cl}$ (Eq. 6). The error in $f_{CO_2,cl}$ (before the kriging step 6 in Sect. 3) due to uncertainty of the $p_{CO_2,cl}$ trend was therefore estimated for each sample station as ±(2010-year) × 0.3 µatm yr^{-1} and binned by month and in 1° × 1° grid boxes ranged between ±(0.9–5.7) µatm. The error was lowest in the North Atlantic Ocean and in the Pacific Ocean because more cruises were performed there in recent times. The absolute monthly mean extrapolation error over all grid points was estimated at 3.0 ± 0.1 µatm (average over all monthly means ± standard deviation). This implies that if in reality the rate of change since 1991 was 1.8 instead of 1.5 µatm yr^{-1}, our $f_{CO_2,cl}$ would be underestimated by ∼ 3 µatm on average. Recent research has shown that an error of this magnitude, or perhaps greater, is probable, since Takahashi et al. (2014) present an updated oceanic p_{CO_2} trend of 1.9 µatm yr^{-1} observed during the 20-year period 1993–2012, a value supported by McKinley et al. (2011).

5.6 Inversion error

Our conversion of $f_{CO_2,is}$ to $p_{CO_2}(T_{eq})$ could introduce an error if the data was not based on x_{CO_2} analysis (cruise flags not A or B), but on f_{CO_2} calculated from a spectrophotometer (very few cruises; Bakker et al., 2014), or if the investigator only provided $f_{CO_2,is}$ or $p_{CO_2,is}$ and did not use Eq. (A1) to correct for the temperature difference. This error was assessed by calculating the conversion from $f_{CO_2,is}$ to $f_{CO_2,ym,i}$ (Eq. 6) using SST and P_{eq} instead of T_{ym} and $P_{eq,ym}$ (expressed as $f_{CO_2,ym,i=is}$). This conversion would ideally produce the original SOCAT $f_{CO_2,is}$ value. A difference between $f_{CO_2,is}$ and $f_{CO_2,ym,i=is}$ implied that our recomputation differed from the one applied by SOCAT or the investigator and we called this difference averaged over one grid box "inversion error". Note that the error was the same for the measurement year as for the year 2010. This resultant calculated error was a small positive bias between 0 and 4 µatm; mostly near zero in the North Atlantic and several other areas, but with some higher levels in the Southern Ocean. The monthly mean inversion bias over all grid points was 1.0 ± 0.2 µatm (average over all monthly means ± standard deviation).

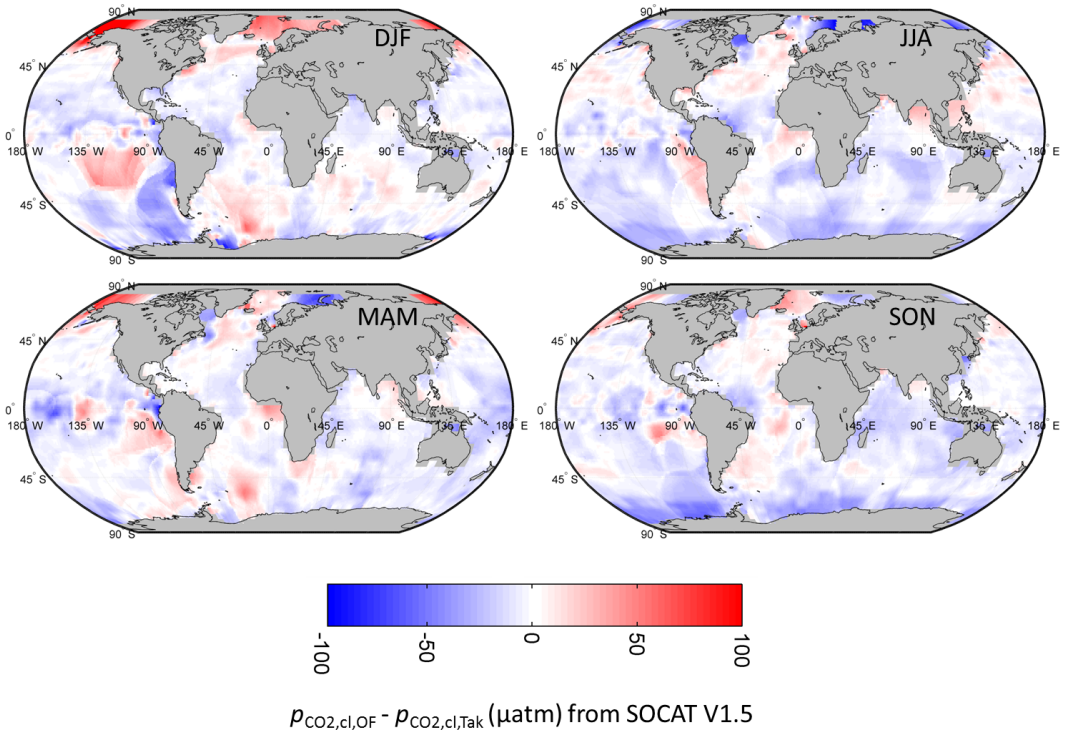

Figure 10. Seasonal differences between OceanFlux $p_{CO_2,cl}$ and $p_{CO_2,cl}$ from Takahashi (2009) normalised to 2010 by adding 15 µatm (= 1.5 µatm yr^{-1} × 10 yr).

5.7 Absent values in our full f_{CO_2} re-computation

A problem related to the inversion error was introduced by absent data in our full f_{CO_2} re-computation (Sect. 3.3). By absent values we mean instances where in situ f_{CO_2} exist in the SOCAT data, but the related instantaneous variables were not measured, or not reported. The impact of these absent values did not always propagate into an inversion error because we made an effort to handle these absent values following SOCAT (Pfeil et al., 2014). For instance, if the in situ salinity or pressure data were not submitted to SOCAT, SOCAT used values from the respectively the World Ocean Atlas 2005 and NCEP for their conversion method. We note that absent values of temperature and pressure at the equilibrator could introduce systematic errors. Over all months and all years the percentages of these absent values were salinity 14 %, T_{eq} 17 %, P 37 %, and P_{eq} 41 %. The $f_{CO_2,ym,i}$ calculations were most sensitive to temperature. If T_{eq} was not provided, we used in situ SST. In that case, the inversion error would be near zero but could lead to significant systematic $f_{CO_2,ym,i}$ errors. We therefore also reproduced our $f_{CO_2,cl}$ distribution maps using only data points with valid T_{eq} values (not shown). These maps appeared to reveal fewer high $f_{CO_2,cl}$ outliers. If only data with valid T_{eq} were selected the data quality was believed to be better, but the number of data points was compromised. Standard deviations calculated with the reduced data set were higher or lower than the standard values, depending on location and month. The monthly mean difference $f_{CO_2,cl}$(all) − $f_{CO_2,cl}$ (valid T_{eq}) ranged between −3.3 µatm (November) and 3.7 µatm (January) and was −0.4 µatm on average over all months. This result illustrates again that both the data sparsity and occasional missing equilibrator temperature data significantly affect the quality of our final f_{CO_2} climatology.

5.8 Measurement errors

Errors in the SOCAT measurements ($f_{CO_2,is}$, T_{eq}, P_{eq} and SST) naturally propagated into $f_{CO_2,cl}$ uncertainty. The total of n independent errors $\pm\Delta x_1, \pm\Delta x_2, \ldots \pm \Delta x_n$ is estimated by $\sqrt{(x_1)^2 + (x_2)^2 + \ldots + (x_n)^2}$. The accuracies for the SOCAT measurements that comply with the Standard Operating Procedures, SOP, criteria (Dickson et al., 2007; Pierrot et al., 2009) are given by Pfeil et al. (2013); these accuracies were the highest that could be expected as not all SOCAT data are of this high standard. Data sets with flags of C and D (59 % in version 1; Bakker et al., 2014) do not meet SOP criteria. (In case of a flag of D the data may meet SOP criteria, but the metadata are incomplete). Likewise, the uncertainty in $T_{ym,i}$ had to be taken into account. Our NetCDF data give the SD values and counts (number of sea surface temperature pixels) with the mean SST_{skin} values from ARC on a 1° × 1° grid. The average standard error, (SD/$\sqrt{\text{count}}$), over all monthly grid boxes that had f_{CO_2} values (all years and

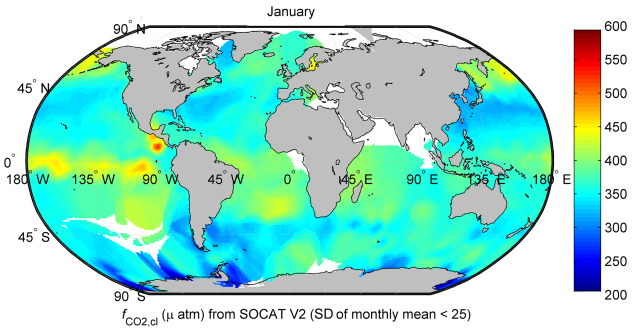

Figure 11. As Fig. 8 but using SOCAT version 2 data.

Table 4. Error estimations of the parameters involved in the $f_{CO_2,cl}$ computation and their consequent errors $\Delta f_{CO_2,cl}$ (µatm).

Parameter x	Unit	Error	$\Delta f_{CO_2,cl}$
ΔSST	°C	±0.05*	±0.75
ΔT_{eq}	°C	±0.05*	±0.015
ΔP_{eq}	hPa	±0.5*	∼0
$\Delta f_{CO_2,is}$	µatm	±2*	±2
$\Delta T_{ym,i}$	K or °C	±0.2	±3

* For SOP data (Pfeil et al., 2013).

months) was ±0.17 K. The uncertainty in the SST difference with subskin SST is ±0.1 K (Donlon et al., 1999). The total uncertainty in $T_{ym,i}$ was therefore estimated to be ±0.2 K ($(\sqrt{0.17^2+0.1^2})$). We estimated the propagation of these errors by applying the error for each parameter, x, and recalculating $f_{CO_2,cl}$. (We calculated $f_{CO_2,cl}$ for the upper limit, $x+\Delta x$, and lower limit, $x-\Delta x$, and calculated the mean of the half of the resulting $f_{CO_2,cl}$ difference, $\Delta f_{CO_2,cl} = \text{mean}\{(f_{CO_2,cl}(x+\Delta x) - f_{CO_2,cl}(x-\Delta x))/2\}$. The results are listed in Table 4. The total error caused by known uncertainties in the parameters was estimated to be > 3.7 µatm ($\sqrt{0.75^2+0.015^2+2^2+3^2}$).

5.9 Summary of errors

The standard deviations produced by the kriging method (Sect. 5.2) are a function of both spatial variation of the data points and random errors in the $f_{CO_2,cl}$ values. The errors caused by the uncertainty of the rate of p_{CO_2} change (temporal extrapolation error) and measurement errors are such random $f_{CO_2,cl}$ errors but the magnitude of their propagation in the kriging procedure is difficult to calculate. Their monthly averages were estimated at ±3.0 µatm (Sect. 5.5) and ±3.7 µatm (Sect. 5.8) respectively and their total 4.8 µatm ($\sqrt{3.0^2+3.7^2}$). Note that an error of 4.8 µatm is smaller than the average monthly minimum SD of the prediction of 6.3 ± 2.6 µatm (Sect. 5.2). The above analysis shows that the SD of the prediction (termed error) was dominated by the spatial variation of the data, an issue that is closely linked to data density (or sparsity). If we use the standard deviation of the kriging as an estimate of the prediction error, the prediction error of $f_{CO_2,cl}$ in a single grid cell ranged between ∼6 and ∼50 µatm and was ∼20 µatm average.

We estimated a bias of ∼1 µatm, introduced by the inversion step in the $f_{CO_2,is}$ to $f_{CO_2,ym,i}$ conversion (Sect. 5.6). The mean $f_{CO_2,cl}$ over all months had a bias of −0.4 µatm due to absent SOCAT values (Salinity, T_{eq}, P and P_{eq}) in the re-computation (Sect. 5.7), so for the total bias of an annual average $f_{CO_2,cl}$ we estimate a value of ∼0.6 µatm. This is less than the systematic bias in the global mean mean surface water p_{CO_2} of about 1.3 µatm as estimated by Takahashi et al. (2009) due to under sampling and their interpolation. The total bias in $f_{CO_2,cl}$ was dominated by the propagation of the uncertainty in the $p_{CO_2,cl}$ trend of ±3 µatm. Notice that the errors could be larger or smaller for individual months or regions. The difference between $f_{CO_2,ym,i}$ and $f_{CO_2,is}$ averaged over all years and grid boxes is relatively small (−1.21 µatm) compared to the uncertainty and biases in the $f_{CO_2,cl}$ estimations, and the consequence of our f_{CO_2} correction may not be large for calculation of the global mean climatological value of f_{CO_2}. However, the standard deviation of the mean difference, ±9.36 µatm, is not small and there are areas and periods where the bias is significant, especially when the sample density is high. The analysis of SST differences in Sect. 1.4 suggests that the original in situ temperatures, and therefore in situ f_{CO_2} values, are biased and that bias strongly varies spatially and seasonally. For regional and seasonal studies our conversion could therefore be much more relevant.

In summary, it is clear that prediction errors are generally dominated by the effects of sparse sampling for most regions and seasons. Note that value of standard deviation in Fig. A4 varies from 5 to 57 µatm. Some of the prediction errors exceed 25 µatm and it is doubtful if the product is useful in those regions and seasons. Note that while other methods do not have such large explicit errors, it is possible that their true error is similar or greater, but that the error is obscured by a false assumption. Our method has the advantage that the problem with sparse sampling is explicit. The only reliable solution is better sampling and it is worth noting that the inclusion of new data in SOCAT v2 yields definite improvements (see next section). The most significant of the other sources of random errors are apparent from Table 4. The propagation of errors within the computation of $f_{CO_2,cl}$ prior to temporal extrapolation and kriging, is described in Sect. 5.8 and based on measurement errors estimated in Table 4. Note that the errors in $f_{CO_2,is}$ and $T_{ym,i}$ are the most significant. The total random error in each calculation of $f_{CO_2,cl}$ is estimated at > ∼3.7 µatm in Sect. 5.8. That error will contribute significantly to the prediction error in some of the better sampled regions. The systematic bias in measurements is relatively low and will result in only a small

systematic global bias in $f_{CO_2,cl}$ ($< \sim 1$ µatm). However, the assumed oceanic p_{CO_2} trend may be a greater source of systematic bias (perhaps 3 µatm), but that bias is difficult to put a firm value on without further study.

6 SOCAT version 2

The addition of new data points and the omission of bad and questionable data (Bakker et al., 2014) gave smoother global distributions and smaller prediction errors (Figs. 11 and A4–A6). The monthly average of the SD of the prediction was 17 ± 3 µatm (in comparison to 20 ± 5 µatm for version 1.5). A few specific regions show a definite improvement. For example, the prediction errors for the southwestern Pacific in DJF and MAM are greatly reduced between Figs. A4 and A6. The monthly mean difference $f_{CO_2,cl}$(v1.5) − $f_{CO_2,cl}$(v2) ranged between −1.1 µatm (January) and 2.4 µatm (July) and was 0.3 µatm on average. Our climatology based on SOCAT version 2 data, reprocessed in a similar manner as the SOCAT version 1.5 data, has also been made available with this paper.

7 Conclusions

We have combined SOCAT in situ data sets with a climate-quality SST data set (ARC) to produce consistent sets of SST and CO_2 parameters suitable for climate change research of air–sea gas exchange. The f_{CO_2} (and p_{CO_2}) predictions and standard deviations are computed for the year 2010 and interpolated to a global $1° \times 1°$ grid, and have been made available together with other climatological data necessary to calculate global oceanic CO_2 fluxes. Two climatology data sets are presented as an online supplement to this paper, each consisting of 12 monthly NetCDF files: one using all SOCAT v1.5 data and one using all data of the recent update SOCAT v2. We identified and calculated various possible errors. The random errors due to the spatial interpolation, closely related to data density, dominated, but all errors vary spatially. The data quality/density in the North Atlantic and North Pacific proved to be superior, and thus these regions have the lowest prediction errors (~ 6 µatm in the best sampled areas). The products have been verified by checking that key and established features such as the seasonal amplitude in the North Atlantic and North Pacific are similar to those reported in other studies. Other regions show much larger prediction errors (often exceeding 25 µatm), highlighting the issue of insufficient sampling. Other interpolation methods may yield nominally lower prediction errors, but that may only obscure the issue of sparse sampling. If we use the standard deviation of the kriging to calculate the prediction error, the prediction error of $f_{CO_2,cl}$ in a single grid cell ranged between ~ 6 and ~ 50 µatm and was ~ 20 µatm on average.

Our products are referenced to a particular year (2010), but can be corrected to a reasonable estimate for another year by reapplying the assumed trend in oceanic p_{CO_2} (1.5 µatm yr^{-1}). The necessity of using multi-year in situ oceanic CO_2 data to supply adequate data for global calculations is invidious; it would be preferable to make genuine single-year calculations. The bias uncertainty in $f_{CO_2,cl}$ was dominated by the assumed value of the oceanic p_{CO_2} trend, which might introduce a systematic global bias of about ±3 µatm into the 2010 products.

Our data set based on SOCAT version 2 is very similar to that derived from SOCAT version 1.5. However, we recommend that users exploit the version that is based on SOCAT version 2, as it is derived from a larger in situ data set and higher quality data. SOCAT asks all data providers to include T_{eq} in their data submission. The absence of equilibrator temperatures from some data sets submitted to SOCAT is unfortunate. It would benefit climatological applications if the equilibrator temperature and f_{CO_2} at the equilibrator temperature was always included in future versions of SOCAT, negating the need for the inversion step described in this paper. Conversion between the temperature of sea water in the equilibrator and a monthly composite temperature from a global, long-term, homogenous, highly stable SST data set such as ARC (Eqs. 5 and 6) could also be included as an additional parameter to provide another standard product in parallel with the direct in situ products.

Appendix A

A1 Descriptions of the different parameters

Table A1. Definitions of the different parameters used in the calculations throughout this paper.

Name	Unit	Meaning
p_{CO_2}	µatm	Partial pressure of CO_2 in seawater
f_{CO_2}	µatm	p_{CO_2} adjusted to account for the fact that the gas is not ideal regarding molecular interactions between the gas and the air
$x_{CO_2,dry}$	ppm	Mole fraction of CO_2 in dry air
$x_{CO_2,wet}$	ppm	Mole fraction of CO_2 in wet air (100 % humidity)
S		Salinity
SST	°C or K	Sea surface temperature in general, and in situ measurement of water temperature at depth by SOCAT if not stated otherwise.
SST_{skin}	K	SST at the sea surface skin (Fig. 1). In this paper represented by monthly $1° \times 1°$ grid-box average of SST_{skin} derived from the ARC data set (Merchant et al., 2012) without differentiating between day- and night-time measurements.
SST_{MBL}	°C or K	SST at the bottom of the mass boundary layer (Fig. 1)
$SST_{subskin}$	K	SST at the bottom of the thermal skin (Fig. 1); in this paper estimated by $SST_{skin} + 0.14$
SST_{depth}	°C or K[a]	SST in metres below the surface (Fig. 1). In this paper represented by SOCAT's in situ measurement.
$SST_{5\,m}$	°C or K[a]	SST at 5 m water depth
T_{ym}	K	Monthly $1° \times 1°$ grid box mean of $SST_{subskin}$
dT	K	$dT = T_{ym}$ – corresponding grid box mean of SOCAT's instantaneous in situ SST measurements
T_{eq}	°C or K	Temperature in the equilibrator chamber
P_{eq}	atm[b]	Pressure in the equilibrator chamber
P_w	atm[b]	Water vapour pressure at T_{eq}
P_{atm}	atm[b]	Atmospheric pressure

[a] In SOCAT regional synthesis files: °C. [b] In SOCAT regional synthesis files: hPa.

Table A2. Definitions of the different indices.

Name	Meaning
ym	For year "y" and month "m"
i	For SOCAT sample point location "*i*"
cl	Climatological value for year 2010
is	In situ

A2 The SOCAT computation of SOCAT fugacity in seawater

The collected CO_2 concentrations are expressed as mole fraction, x_{CO_2}, partial pressure, p_{CO_2}, or fugacity, f_{CO_2}, of CO_2. SOCAT's re-computation is to achieve a uniform representation of the CO_2 measurements and all measurements are converted to fugacity in seawater $f_{CO_2,is}$ (fCO2_rec) for in situ sea surface, SST (temp). The parameters in brackets refer to their SOCAT version 1.5 names (Pfeil and Olsen, 2009). SST is the intake temperature which signifies SST_{depth}. The shipboard measurements were taken at equilibrator temperature T_{eq} (Temperature_equi) and equilibrator pressure, P_{eq} (Pressure_equi). SOCAT calculates $f_{CO_2,is}$ from $p_{CO_2,is}$, partial pressure in seawater corrected for the difference between SST and the temperature at the equilibrator, using Eqs. (A1) and (A2)

$$p_{CO_2,is} = p_{CO_2}(T_{eq}) \exp\left(0.0423(SST - T_{eq})\right) \quad (A1)$$

(Takahashi et al., 1993)

$$f_{CO_2,is} = p_{CO_2,is} \exp \left(\frac{\left[B(CO_2, SST) + 2(1 - x_{CO_2,wet}(T_{eq}))^2 \delta(CO_2, SST)\right] P_{eq}}{R \cdot SST} \right) \quad (A2)$$

with $B(CO_2, SST)$ ($cm^3\,mol^{-1}$) and $\delta(CO_2, SST)$ ($cm^3\,mol^{-1}$) calculated from Weiss (1974):

$$B(CO_2, T) = -1636.75 + 12.0408\,T - 3.27957 \times 10^{-2} T^2 + 3.16528 \times 10^{-5} T^3 \quad (A3)$$

$$\delta(CO_2, T) = 57.7 - 0.118\,T \quad (A4)$$

(Pfeil et al., 2013). In Eqs. (A1)–(A4) temperatures are in K, P_{eq} in atm, and $x_{CO_2,wet}(T_{eq})$ is the wet mole fraction as parts per million (ppm) of CO_2 at equilibrator temperature. How $p_{CO_2}(T_{eq})$ is measured and the temperature correction (Eq. A1) are discussed in respective Sects. 2.2 and 2.3.

Different measured parameters are available in different records to use as starting point for the SOCAT recomputation of $f_{CO_2,is}$ and the conversions from x_{CO_2} and p_{CO_2} are carried out using a clear hierarchy for the preferred CO_2 input parameter (Table 4 in Pfeil et al., 2013). Therefore SOCAT applies the following strict guidelines:

1. recalculate f_{CO_2} whenever possible;
2. order of preference of the starting point is: x_{CO_2}, p_{CO_2}, f_{CO_2};
3. minimise the use of external data.

The majority of the cases (57.5%) is derived from $x_{CO_2,wet}(T_{eq})$. However, in many cases only $f_{CO_2,is}$ (8.4%) or $p_{CO_2,is}$ (13.8 %) was provided so that it is not certain that Eq. (A1) was used by the cruise scientists to convert $p_{CO_2}(T_{eq})$ to $p_{CO_2,is}$. Moreover, if only $f_{CO_2,is}$ was reported, but pressure and salinity were not, $f_{CO_2,is}$ is not recalculated and $f_{CO_2,is}$ is taken as provided. The regional synthesis files only contain recomputed $f_{CO_2,is}$ values and don't give direct information about starting points other than which one was used (fCO2_source). However, each record contains a field "doi", indicating the digital object identifier to a publically accessible online data file in the PANGAEA database (http://www.pangaea.de/) where the original measurements before re-computation can be found. The individual cruise data files also contain various x_{CO_2}, p_{CO_2}, and f_{CO_2} data (Table 5 in Pfeil et al., 2013). Because we wanted to use SOCAT's uniform database, and not re-create it, we estimated $f_{CO_2,cl}$ from the $f_{CO_2,is}$ values in the merged synthesis files as explained in Sect. 3. An estimation of the errors in recomputed $f_{CO_2,cl}$ due to varying starting points is given in Sects. 5.6 and 5.7.

A3 Inversion: Conversion of $f_{CO_2,is}$ to p_{CO_2} (T_{eq})

First $p_{CO_2,is}$ (µatm) was derived from $f_{CO_2,is}$ (µatm) by inverting Eq. (A2):

$$p_{CO_2,is} = f_{CO_2,is} \exp \left(-\frac{\left[B + 2\left(1 - x_{CO_2,wet}(T_{eq})\right)^2 \delta\right] P_{eq}}{R \cdot SST} \right) \quad (A5)$$

with $B = B(CO_2, SST)$ and $\delta = \delta(CO_2, SST)$ both in ($cm^3\,mol^{-1}$) from respective Eqs. (A3) and (A4) with SST and T_{eq} in K and P_{eq} in atm. The gas constant $R = 82.0578\,cm^3\,atm\,mol^{-1}\,K^{-1}$. Defining $x_{CO_2,wet}(T_{eq})$ as $p_{CO_2}(T_{eq})/P_{eq}$ (Eq. 3) and writing $p_{CO_2}(T_{eq})$ in terms of $p_{CO_2,is}$ (Eq. A1), Eq. (A5) leads to

$$p_{CO_2,is} = f_{CO_2,is} \exp \left(-\frac{\left[B + 2\left(1 - \frac{p_{CO_2,is} \exp(-0.0423(SST - T_{eq}))}{P_{eq}}\right)^2 \delta\right] P_{eq}}{R \cdot SST} \right) \quad (A6)$$

Eq. (A6) was solved with an iterative calculation

$$\left[p_{CO_2,is}\right]_{n+1} = f_{CO_2,is} \exp\left(g\left(\left[p_{CO_2,is}\right]_n, SST, T_{eq}, P_{eq}\right)\right) \quad (A7)$$

(with g a function describing the exponent). In the first iteration the initial guess of $[p_{CO_2,is}]_1$ was $f_{CO_2,is}$ and the result $[p_{CO_2,is}]_2$ was put back in the right hand side of Eq. (A7). This step was repeated until $[p_{CO_2,is}]_N - [p_{CO_2,is}]_{N-1} < 2^{-52}$. Using Eq. (A1) we could then estimate the original $p_{CO_2}(T_{eq})$,

$$p_{CO_2}(T_{eq}) = p_{CO_2,is} \exp\left(-0.0423(SST - T_{eq})\right) \quad (A8)$$

A4 Spatial interpolation errors in estimations of $f_{CO_2,cl}$ in 2010

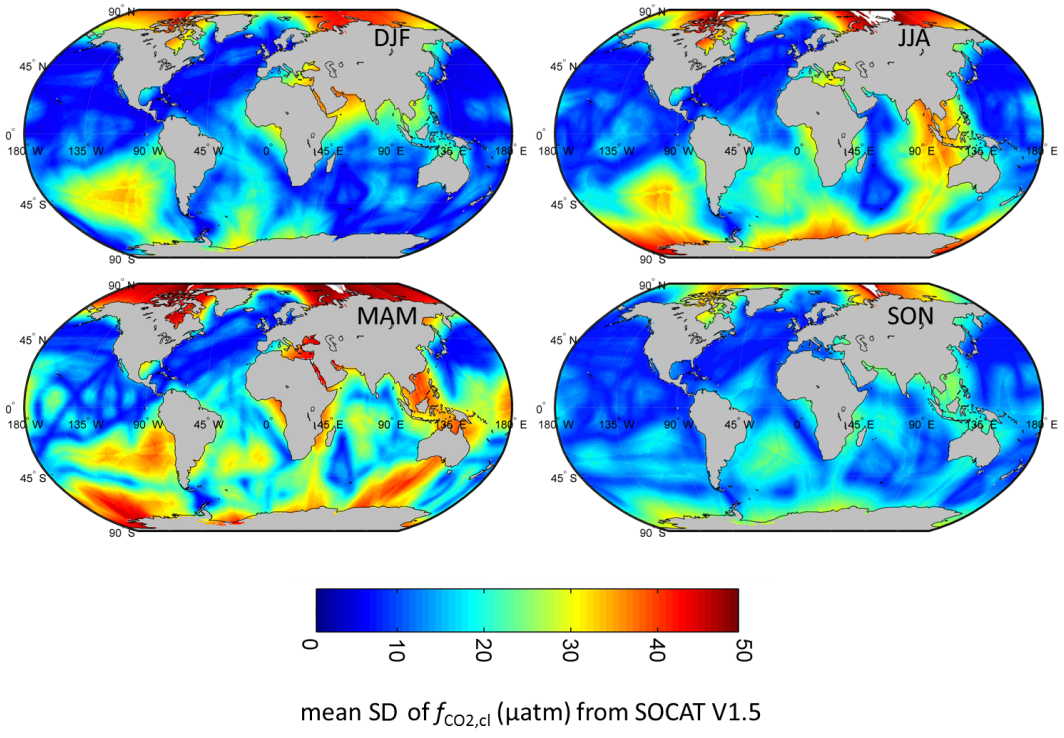

Figure A1. Seasonal SD values in $f_{CO_2,cl}$ (µatm) estimated for 2010 in DJF (December–February), MAM (March–May), JJA (July–August) and SON (September–November) on a 0–50 µatm scale; grid-box values as shown in Fig. 8 for January were averaged over the 3 months.

A5 Seasonal global distributions of $f_{CO_2,cl}$ in 2010 from SOCAT version 2

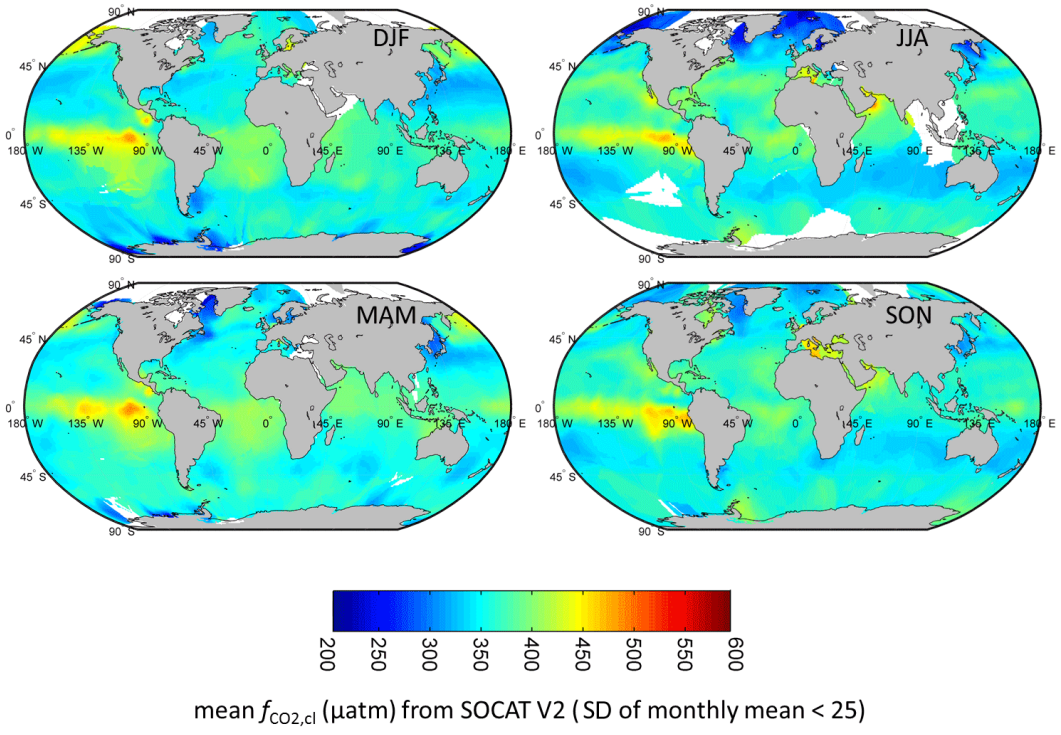

Figure A2. As Fig. 9 but for SOCAT version 2 instead of version 1.5.

A6 Spatial interpolation errors in $f_{CO_2,cl}$ in 2010 using SOCAT version 2

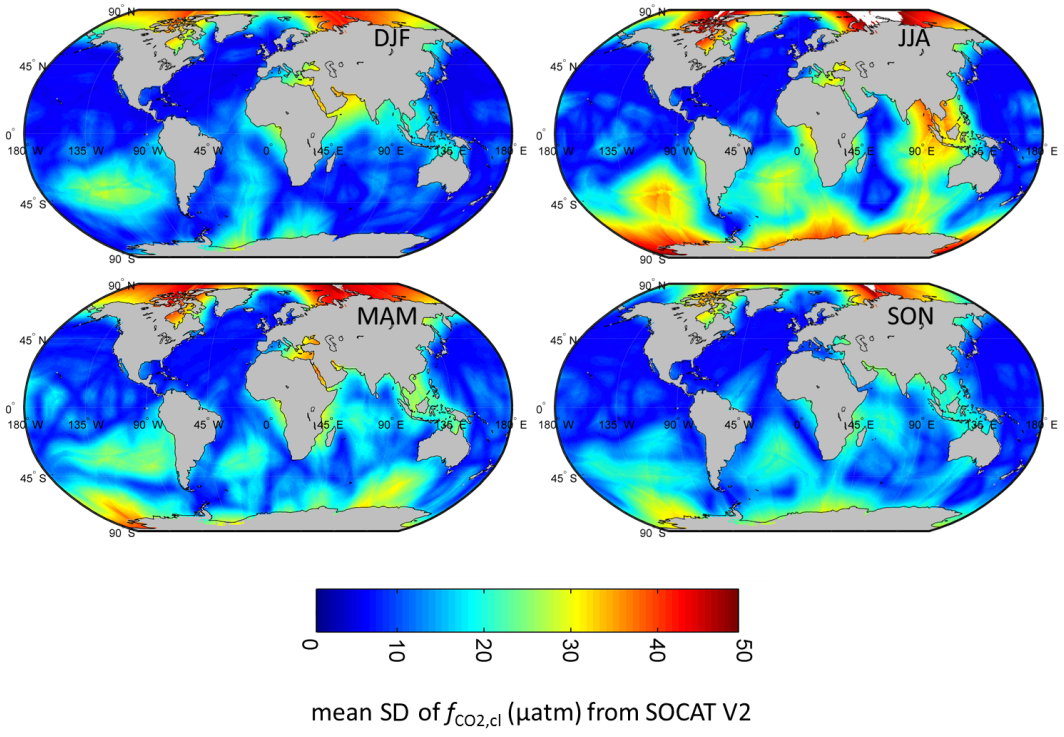

Figure A3. As Fig. A4 but for SOCAT version 2 instead of version 1.5.

The Supplement related to this article is available online at doi:10.5194/os-11-519-2015-supplement.

Acknowledgements. This research is a contribution of the National Centre for Earth Observation, a NERC Collaborative Centre and was supported by the European Space Agency (ESA) Support to Science Element (STSE) project OceanFlux Greenhouse Gases (contract number 4000104762/11/I-AM). We are grateful for access to SOCAT data. The Surface Ocean CO_2 Atlas (SOCAT) is an international effort, supported by the International Ocean Carbon Coordination Project (IOCCP), the Surface Ocean Lower Atmosphere Study (SOLAS), and the Integrated Marine Biogeochemistry and Ecosystem Research program (IMBER), to deliver a uniformly quality-controlled surface-ocean CO_2 database. The many researchers and funding agencies responsible for the collection of data and quality control are thanked for their contributions to SOCAT. The authors also thank the NERC Earth Observation Data Acquisition and Analysis Service (NEODAAS) for supplying data for this study.

Edited by: C. Garbe

References

Bakker, D. C. E., Pfeil, B., Smith, K., Hankin, S., Olsen, A., Alin, S. R., Cosca, C., Harasawa, S., Kozyr, A., Nojiri, Y., O'Brien, K. M., Schuster, U., Telszewski, M., Tilbrook, B., Wada, C., Akl, J., Barbero, L., Bates, N. R., Boutin, J., Bozec, Y., Cai, W.-J., Castle, R. D., Chavez, F. P., Chen, L., Chierici, M., Currie, K., de Baar, H. J. W., Evans, W., Feely, R. A., Fransson, A., Gao, Z., Hales, B., Hardman-Mountford, N. J., Hoppema, M., Huang, W.-J., Hunt, C. W., Huss, B., Ichikawa, T., Johannessen, T., Jones, E. M., Jones, S. D., Jutterström, S., Kitidis, V., Körtzinger, A., Landschützer, P., Lauvset, S. K., Lefèvre, N., Manke, A. B., Mathis, J. T., Merlivat, L., Metzl, N., Murata, A., Newberger, T., Omar, A. M., Ono, T., Park, G.-H., Paterson, K., Pierrot, D., Ríos, A. F., Sabine, C. L., Saito, S., Salisbury, J., Sarma, V. V. S. S., Schlitzer, R., Sieger, R., Skjelvan, I., Steinhoff, T., Sullivan, K. F., Sun, H., Sutton, A. J., Suzuki, T., Sweeney, C., Takahashi, T., Tjiputra, J., Tsurushima, N., van Heuven, S. M. A. C., Vandemark, D., Vlahos, P., Wallace, D. W. R., Wanninkhof, R., and Watson, A. J.: An update to the Surface Ocean CO_2 Atlas (SOCAT version 2), Earth Syst. Sci. Data, 6, 69–90, doi:10.5194/essd-6-69-2014, 2014.

Dlugokencky, E. J., Masarie, K. A., Lang, P. M., and Tans, P. P.: NOAA Greenhouse Gas Reference from Atmospheric Carbon Dioxide Dry Air Mole Fractions from the NOAA ESRL Carbon Cycle Cooperative Global Air Sampling Network, available at: ftp://aftp.cmdl.noaa.gov/data/trace_gases/co2/flask/surface/ (last access: 27 July 2014), 2014.

Dickson, A. G., Sabine, C. L., and Christian, J. R. (Eds.): Guide to best practices for ocean CO_2 measurements, PICES Special Publication 3, IOCCP Report, 8, 191 pp., 2007.

Donlon, C. J., Nightingale, P. D., Sheasby, T., Turner, J., Robinson, I. S., and Emery, J.: Implications of the oceanic thermal skin temperature deviation at high wind speeds, Geophys. Res. Lett., 26, 2505–2508, 1999.

Donlon, C. J., Minnett, P., Gentemann, C., Nightingale, T. J., Barton, I. J., Ward, B., and Murray, J.: Towards improved validation of satellite sea surface skin temperature measurements for climate research, J. Climate, 15, 353–369, 2002.

Donlon, C., Robinson, I., Casey, K. S., Vazquez-Cuervo, J., Armstrong, E., Arino, O., Gentemann, C., May, D., Leborgne, P., Piollé, J., Barton, I., Beggs, H., Poulter, D. J. S., Merchant, C. J., Bingham, A., Heinz, S., Harris, A., Wick, G., Emery, B., Minnett, P., Evans, R., Llewwellyn-Jones, D., Mutlow, C., Reynolds, R. W., Kawamura, H., and Rayner, N.: The GODAE High Resolution Sea Surface Temperature Pilot Project (GHRSST-PP), B. Am. Meteorol. Soc., 88, 1197–1213, 2007.

Emery, W. J., Cherkauer, K., Shannon, B., and Reynolds, R. W.: Hull-mounted sea surface temperatures from ships of opportunity, J. Atmos. Ocean. Tech., 14, 1237–1251, doi:10.1175/1520-0426(1997)014<1237:HMSSTF>2.0.CO;2, 1997.

Emery, W. J., Baldwin, D. J., Schlüssel, P., and Reynolds, R. W.: Accuracy of in situ sea surface temperatures used to calibrate infrared satellite measurements, J. Geophys. Res., 106, 2387–2405, doi:10.1029/2000JC000246, 2001.

Fangohr, S. and Woolf, D. K.: Application of new parameterization of gas transfer velocity and their impact on regional and global marine CO_2 budgets, J. Marine Syst., 66, 195–203, 2007.

Jeffery, C. D., Woolf, D. K., Robinson, I. S., and Donlon, C. J.: One-dimensional modelling of convective CO_2 exchange in the Tropical Atlantic, Ocean Model., 19, 161–182, 2007.

Jeffery, C. D., Robinson, I., Woolf, D. K., and Donlon, C. J.: The response to phase-dependent wind stress and cloud fraction of the diurnal cycle of SST and air–sea CO_2 exchange, Ocean Model., 23, 33–48, 2008.

Jones, S. D., Le Quéré, C., and Rödenbeck, C.: Autocorrelation characteristics of surface ocean $pCO_2$and air-sea CO_2 fluxes, Global Biochem. Cy., 26, GB2042, doi:10.1029/2010GB004017, 2012.

Kawai, Y. and Wada, A.: Diurnal sea surface temperature variation and its impact on the atmosphere and ocean: a review, J. Oceanogr., 63, 721–744, 2007.

Kennedy, J. J.: A review of uncertainty in in situ measurements and data sets of sea surface temperature, Rev. Geophys., 51, 1–32, doi:10.1002/2013RG000434, 2013.

Kennedy, J. J., Rayner, N. A., Smith, R. O., Saunby, M., and Parker, D. E.: Reassessing biases and other uncertainties in sea-surface temperature observations since 1850 Part 1: Measurement and sampling errors, J. Geophys. Res., 116, D14103, doi:10.1029/2010JD015218, 2011a.

Kennedy, J. J., Rayner, N. A., Smith, R. O., Saunby, M., and Parker, D. E.: Reassessing biases and other uncertainties in sea-surface temperature observations since 1850 Part 2: Biases and homogenisation, J. Geophys. Res., 116, D14104, doi:10.1029/2010JD015220, 2011b.

Kent, E. C., Taylor, P. K., Truscott, B. S., and Hopkins, J. A.: The accuracy of voluntary observing ship's meteorological observations, J. Atmos. Ocean. Tech., 10, 591–608, 1993.

Kettle, H., Merchant, C. J., Jeffery, C. D., Filipiak, M. J., and Gentemann, C. L.: The impact of diurnal variability in sea surface temperature on the central Atlantic air-sea CO_2 flux, Atmos. Chem. Phys., 9, 529–541, doi:10.5194/acp-9-529-2009, 2009.

Land, P. E., Shutler, J. D., Cowling, R. D., Woolf, D. K., Walker, P., Findlay, H. S., Upstill-Goddard, R. C., and Donlon, C. J.: Climate change impacts on sea–air fluxes of CO_2 in three Arctic seas: a sensitivity study using Earth observation, Biogeosciences, 10, 8109–8128, doi:10.5194/bg-10-8109-2013, 2013.

Landschützer, P., Gruber, N., Bakker, D. C. E., Schuster, U., Nakaoka, S., Payne, M. R., Sasse, T. P., and Zeng, J.: A neural network-based estimate of the seasonal to inter-annual variability of the Atlantic Ocean carbon sink, Biogeosciences, 10, 7793–7815, doi:10.5194/bg-10-7793-2013, 2013.

Liss, P. S. and Merlivat, L.: Air-sea gas exchange rates: introduction and synthesis, in: The Role of Air–Sea Exchange in Geochemical Cycling, edited by: Buat-Menard, P., D Reidel, 113–127, 1986.

McKinley, G. A., Fay, A. R., Takahashi, T., and Metzl, N.: Convergence of atmospheric and North Atlantic carbon dioxide trends on multidecadal timescales, Nat. Geosci., 4, 606–619, doi:10.1038/NGEO1193, 2011.

Merchant, C. J., Llewellyn-Jones, D., Saunders, R. W., Rayner, N. A., Kent, E. C., Old, C. P., Berry, D., Birks, A. R., Blackmore, T., Corlett, G. K., Embury, O., Jay, V. L., Kennedy, J., Mutlow, C. T., Nightingale, T. J., O'Carroll, A. G., Pritchard, M. J., Remedios, J. J., and Tett, S.: Deriving a sea surface temperature record suitable for climate change research from the along-track scanning radiometers, Adv. Space Res., 41, 1–11, 2008.

Merchant, C. M., Embury, O., Rayner, N. A., David, I., Berry, D. I., Corlett, G. K., Lean, K., Veal, K. L., Kent, E. C., Llewellyn-Jones, D. T., Remedios, J. J., and Saunders, R.: A 20 year independent record of sea surface temperature for climate from Along-Track Scanning Radiometers, J. Geophys. Res., 117, C12013, doi:10.1029/2012JC008400, 2012.

Pierrot, D., Neill, C., Sullivan, K., Castle, R., Wanninkhof, R., Lüger, H., Johannessen, T., Olsen, A., Feely, R. A., and Cosca, C. E.: Recommendations for autonomous underway p_{CO_2} measuring systems and data reduction routines, Deep-Sea Res. Pt. II, 56, 512–522, doi:10.1016/j.dsr2.2008.12.005, 2009.

O'Carroll, A. G., Eyre, J. R., and Saunders, R. W.: Three-way error analysis between AATSR, AMSR-E, and in situ sea surface temperature observations, J. Atmos. Ocean. Tech., 25, 1197–1207, doi:10.1175/2007JTECHO542.1, 2008.

Olsen, A., Omar, A. M., Stuart-Menteth, A. C., and Trinanes, J. A.: Diurnal variations of surface ocean pCO_2 and sea-air CO_2 flux evaluated using remotely sensed data, Geophys. Res. Lett., 31, L20304, doi:10.1029/2004GL020583, 2004.

Pebesma, E. J.: Gstat's User Manual, available at: http://www.gstat.org/gstat.pdf (last access: 27 February 2013), 1–100, 1999.

Pebesma, E. J.: Multivariable geostatistics in S: the gstat package, Comput. Geosci., 30, 683–691, 2004.

Pfeil, B. and Olsen, A.: A uniform format surface fCO_2 database, available at: http://www.socat.info/publications.html (last access: 04 June 2012), 1–9, 2009.

Pfeil, B., Olsen, A., Bakker, D. C. E., Hankin, S., Koyuk, H., Kozyr, A., Malczyk, J., Manke, A., Metzl, N., Sabine, C. L., Akl, J., Alin, S. R., Bates, N., Bellerby, R. G. J., Borges, A., Boutin, J., Brown, P. J., Cai, W.-J., Chavez, F. P., Chen, A., Cosca, C., Fassbender, A. J., Feely, R. A., González-Dávila, M., Goyet, C., Hales, B., Hardman-Mountford, N., Heinze, C., Hood, M., Hoppema, M., Hunt, C. W., Hydes, D., Ishii, M., Johannessen, T., Jones, S. D., Key, R. M., Körtzinger, A., Landschützer, P., Lauvset, S. K., Lefèvre, N., Lenton, A., Lourantou, A., Merlivat, L., Midorikawa, T., Mintrop, L., Miyazaki, C., Murata, A., Nakadate, A., Nakano, Y., Nakaoka, S., Nojiri, Y., Omar, A. M., Padin, X. A., Park, G.-H., Paterson, K., Perez, F. F., Pierrot, D., Poisson, A., Ríos, A. F., Santana-Casiano, J. M., Salisbury, J., Sarma, V. V. S. S., Schlitzer, R., Schneider, B., Schuster, U., Sieger, R., Skjelvan, I., Steinhoff, T., Suzuki, T., Takahashi, T., Tedesco, K., Telszewski, M., Thomas, H., Tilbrook, B., Tjiputra, J., Vandemark, D., Veness, T., Wanninkhof, R., Watson, A. J., Weiss, R., Wong, C. S., and Yoshikawa-Inoue, H.: A uniform, quality controlled Surface Ocean CO2 Atlas (SOCAT), Earth Syst. Sci. Data, 5, 125–143, doi:10.5194/essd-5-125-2013, 2013.

Reynolds, R. W., Gentemann, C. L., and Corlett, G. K.: Evaluation of AATSR and TMI satellite SST data, J. Climate, 23, 152–165, doi:10.1175/2009JCLI3252.1, 2010.

Robertson, J. E. and Watson, A. J.: Thermal skin effect of the surface ocean and its implications for CO_2 uptake, Nature, 358, 738–740, 1992.

Rödenbeck, C., Keeling, R. F., Bakker, D. C. E., Metzl, N., Olsen, A., Sabine, C., and Heimann, M.: Global surface-ocean pCO_2 and sea-air CO_2 flux variability from an observation-driven ocean mixed-layer scheme, Ocean Sci., 9, 193–216, doi:10.5194/os-9-193-2013, 2013.

Sabine, C. L., Hankin, S., Koyuk, H., Bakker, D. C. E., Pfeil, B., Olsen, A., Metzl, N., Kozyr, A., Fassbender, A., Manke, A., Malczyk, J., Akl, J., Alin, S. R., Bellerby, R. G. J., Borges, A., Boutin, J., Brown, P. J., Cai, W.-J., Chavez, F. P., Chen, A., Cosca, C., Feely, R. A., González-Dávila, M., Goyet, C., Hardman-Mountford, N., Heinze, C., Hoppema, M., Hunt, C. W., Hydes, D., Ishii, M., Johannessen, T., Key, R. M., Körtzinger, A., Landschützer, P., Lauvset, S. K., Lefèvre, N., Lenton, A., Lourantou, A., Merlivat, L., Midorikawa, T., Mintrop, L., Miyazaki, C., Murata, A., Nakadate, A., Nakano, Y., Nakaoka, S., Nojiri, Y., Omar, A. M., Padin, X. A., Park, G.-H., Paterson, K., Perez, F. F., Pierrot, D., Poisson, A., Ríos, A. F., Salisbury, J., Santana-Casiano, J. M., Sarma, V. V. S. S., Schlitzer, R., Schneider, B., Schuster, U., Sieger, R., Skjelvan, I., Steinhoff, T., Suzuki, T., Takahashi, T., Tedesco, K., Telszewski, M., Thomas, H., Tilbrook, B., Vandemark, D., Veness, T., Watson, A. J., Weiss, R., Wong, C. S., and Yoshikawa-Inoue, H.: Surface Ocean CO_2 Atlas (SOCAT) gridded data products, Earth Syst. Sci. Data, 5, 145–153, doi:10.5194/essd-5-145-2013, 2013.

Schuster, U., Watson, A. J., Bates, N. R., Corbiere, A., Gonzalez-Davila, M., Metzl, N., Pierrot, D., and Santana-Casiano, M.: Trends in North Atlantic sea-surface f_{CO_2} from 1990 to 2006, Deep-Sea Res. II, 56, 620–629, 2009.

Takahashi, T. J., Olafsson, J. G., Goddard, D. W., Chipman, D. W., and Sutherland, S. C.: Seasonal variation of CO_2 and nutrients in the high-latitude surface oceans: A comparative study, Global Biochem. Cy., 7, 843–878, 1993.

Takahashi, T., Sutherland, S. C., Sweeney, C., Poisson, A., Metzl, N., Tilbrook, B., Bates, N., Wanninkhof, R., Feely, R. A., Sabine, C., Olafsson, J., and Nojiri, Y.: Global air–sea CO_2 flux based on climatological surface ocean pCO_2, and seasonal biological and temperature effects, Deep-Sea Res. Pt. II, 45, 1601–1622, 2002.

Takahashi, T., Sutherland, S. C., Wanninkhof, R., Sweeney, C., Feely, R. A., Chipman, D. W., Hales, B., Friederich, G., Chavez, F., Sabine, C., Watson, A., Bakker, D. C. E., Schuster, U., Metzl, N., Yoshikawa-Inoue, H., Ishii, M., Midorikawa, T., Nojiri, Y.,

Körtzinger, A., Steinhoff, T., Hoppema, M., Olafson, J., Arnarson, T. S., Tilbrook, B., Johannesesen, T., Olsen, A., Bellerby, R., Wong, C. S., Delile, B., Bates, N. R., and de Baar, H. J. W.: Climatological mean and decadal change in surface ocean pCO_2, and net sea–air CO_2 flux over the global oceans, Deep-Sea Res. Pt. II, 56, 554–577, 2009.

Takahashi, T., Sutherland, S. C., Chipman, D. W., Goddard, J. G., and Ho, C.: Climatological distributions of pH, pCO_2, total CO_2, alkalinity, and $CaCO_3$ saturation in the global surface Ocean, and temporal changes at selected locations, Mar. Chem., 164, 95–125, doi:10.1016/j.marchem.2014.06.004, 2014.

Wanninkhof, R., Asher, W. E., Ho, D. T., Sweeney, C., and McGillis, W. R.: Advances in quantifying air–sea gas exchange and environmental forcing, Annu. Rev. Mar. Sci., 1, 213–244, doi:10.1146/annurev.marine.010908.163742, 2009.

Ward, B., Wanninkhof, R., McGillis, W. R., Jessup, A. T., DeGrandpre, M. D., Hare, J. E., and Edson, J. B.: Biases in the air–sea flux of CO_2 resulting from ocean surface temperature gradients, J. Geophys. Res., 109, C08S08, doi:10.1029/2003JC001800, 2004.

Weiss, R. F.: Carbon dioxide in water and seawater: the solubility of a non-ideal gas, Mar. Chem., 2, 203–215, 1974.

Wilmott, C. J., Ackleson, S. G., Davis, R. E., Feddema, J. J., Klink, K. M., Legates, D. R., O'Donnell, J., and Rowe, C.: Statistics for the evaluation and comparison of models, J. Geophys. Res., 90, 8995–9005, 1985.